Characterization of Novel Genetic Alleles of Cellulose Synthase

Robert A. Law

Submitted as partial completion of a Masters Degree in Applied Bioscience to:

Supervisor:

Dr. D. Bonetta

Committee members:

Dr. A. Kumar

Dr. J. Strap

Table Of Contents

1.0 Abstract

Cellulose is the most abundant polymer on earth. Despite this, relatively little is known about the proteins and biochemical mechanisms governing cellulose biosynthesis. Only in the past 10 years since the sequencing of the *Arabidopsis thaliana* genome have we begun to unravel the full complexity of this process in plants. A chemical genetics screen using the cellulose biosynthesis herbicide flupoxam was undertaken to identify potentially novel proteins involved in this process. Despite falling short of identifying these new players, six novel mutations were identified on Cellulose Synthase (*CESA)* 1 and 3 leading to flupoxam resistance. Two of these mutations were positionally cloned using Next-Generation Mapping (NGM) technology, while the others were identified using sequencing. The mutations led to both decreased cellulose crystallinity as well as enhanced cellulose hydrolysis. Future research will fully characterize using additional enzymatic hydrolysis methods and gas chromatography. The second aspect of the project involved the development of a membrane yeast two hybrid (MbyTH) for use with primary cell wall cellulose synthases. Paired interaction studies determined that CESA1 interacts strongly with itself. Also, CESA3 interacts strongly with itself. However, interaction between CESA1 and 3 was weak. It is possible that a tertiary protein is required in order for this interaction to occur. Also, a weak interaction between CTL1/Pom1 (Chitinase –like protein 1) was observed with CESA3. An interaction trap using either CESA1 or 3 as bait may elucidate additional proteins involved in the process of cellulose synthesis.

2.0 Introduction

2.1 Cellulose as an emerging prospect for bioethanol production

Cellulose comprises approximately one third the biomass derived from plant matter. It is a β-1,4 linked polymer of glucose, with successive units inverted 180 degrees with respect to each other. The cellulose microfibril is composed of 36 hydrogen bonded chains containing approximately 500-14000 glucose molecules (Somerville, 2006). Many microfibrils in turn provide external resistance to internal turgor pressure, so as to allow a plant to maintain erect growth (Somerville, 2006). Cellulose has historically shown economic importance due to its integral role in the production of materials like textiles, paper and plastics (Li *et al.,* 2008). Of particular importance is the role of cellulose as the major nutritional component of ruminant livestock (Li *et al*., 2008). An emerging industrial prospect for cellulose is its use as a feedstock for bioethanol production. Currently, bioethanol production is limited to the fermentation of starch from maize kernels (Sticklen, 2006). Given the abundance of glucose in plant tissue in the form of cellulose, it is plausible in theory to use this for fermentative ethanol production. However, access to this rich source of sugar is not trivial, given the recalcitrant nature of cellulose to hydrolysis. This is a result of numerous inter and intra-chain hydrogen bonding (Nishiyama *et al*., 2002 and Nishiyama *et al*., 2003). It is also imbedded in a matrix of other polymers including lignin, which specifically impede access via hydrolyzing enzymes (Li *et al*., 2008). There are currently many avenues being pursued as far as improving cellulosic bioethanol for economies of scale. These include modifying the pretreatment processes to better improve the removal of lignin, finding and genetically modifying cellulases needed to break down cellulose, altering cell wall

composition and understanding pathways that govern cellulose production, cell wall integrity, expansion and growth etc. (Sticklin, 2006). Understanding the enzymes responsible for cellulose production is particularly salient since the process can then be manipulated to improve access to cellulose.

2.2 The process of cellulose synthesis and the cellulose synthase (CESA)

The plant cell wall is synthesized in two steps. The primary cell wall is first initiated during the cell division and growth, while the secondary cell wall is initiated after growth has ceased. The primary cell wall is composed primarily of cellulose, hemicellulose, pectin and protein, while the secondary cell wall is more lignin and cellulose rich. Cellulose is synthesized at the plasma membrane via localized cellulose synthase (CESA) proteins, which are part of the glycosyltransferase-2 family of inverting glycosyltransferases (Saxena *et al.,* 2001). The CESA proteins contain a cysteine rich N-terminal zinc finger binding domain implicated in protein- protein interaction through cysteine-cysteine oxidation, a large central domain containing the catalytic motifs D/D/DxD as well as the Q/RxxRW motif (Saxena and Brown, 1997). The QxxRW domain is characteristic of all processive glycosyltransferases and is speculated to be involved in holding the growing glucan chain in place (Saxena *et al*., 2001). The enzymes are termed " inverting" due to the conversion of an α-linked UDP glucose to a β-linkage on the cellulose fibril. Cellulose synthases are believed to catalyze glycosidic linkages using an S_n2 reaction mechanism with the conserved aspartic acid residues coordinating the C4-hydroxyl on the β-1-4 Glucan for nucleophilic attack on the phosphodiester bond of incoming UDP-Glucose monomers (Saxena *et al*., 2001). Large hexameric complexes on the plasma membrane containing at least 36 CESA proteins are believed to catalyze

the cellulose microfibril (Kimura *et al.,* 1999). It is hypothesized that each individual CESA protein is responsible for secreting one cellulose chain with all 36 chains forming an elementary microfibril (Herth, 1983). *Arabidopsis thaliana* contains 10 paralogous CESA genes, which share 64% sequence identity (Richmond, 2000). Loss-of-function (LOF) mutations in *CESA 4, 7* and *8* cause defects in secondary cell wall synthesis while LOF mutations in *CESA 1, 3,* and *6* lead to defects in the production of the primary cell walls (Turner and Somerville, 1997; Desprez *et al.,* 2007). Pull down experiments have shown that CESA 1, 3 and 6 interact in-vivo and in-vitro, but their relative stoichiometry is unknown (Desperez *et al.,* 2007 and Wang *et al.,* 2008). Antisense knockouts of the *CESAs* involved in primary cell wall synthesis show that CESA 1 and 3 are absolutely required for growth (Somerville, 2006). Also, null mutations in either *CESA* 1 or 3 are gametophytic lethal, pointing to their relative individual importance in *Arabidopsis* (Persson *et al.,* 2007). However, while over expression of *CESA* 1 is sufficient to rescue *CESA* 3 knockouts, the same is not true for over expression of *CESA* 3 in a *CESA* 1 mutant background (Burn *et al*., 2002). The role of *CESA* 6 seems dispensable since *CESA* 2 and 5 cDNA expressed in frame with a *CESA* 6 promoter partially rescues *CESA 6* LOF (Desprez *et al.,* 2007; Persson *et al*., 2007) LOF *CESA* 6 mutations such as *prc1-1* exhibit weak phenotypes with reduced length in hypocotyls, attributable to its redundancy with *CESA* 2, -5, and -9 (Desnos *et al.,* 1996; Persson *et al.,* 2005). Given these differences, it is likely that individual subunits have different roles in the complex.

2.3 The use of herbicides to probe molecular basis of cellulose synthesis

Mutant screens have revealed a number of mutations pertinent to cellulose synthesis, including many which map to the *CESAs* with variation in severity (Somerville, 2006). For example, the *rsw1* mutation in *CESA 1* is a temperature sensitive allele which results in the production of amorphous glucan in place of cellulose (Arioli *et al.,* 1998). The *thanatos* mutation is a dominant negative P(578)S substitution in the catalytic region of CESA 3, resulting in reduced growth and cellulose content with homozygote individuals failing to survive to adulthood (Daras *et al*., 2009) Another means of phenotypic analysis is through chemical genetics. Chemicals that disrupt some physiological process can either disrupt the protein responsible for synthesis or the reaction itself. In the context of cellulose synthesis, cellulose-biosynthesis inhibitors (CBIs) are a group of chemically diverse compounds which include: dichlorobenzonitrile, isoxaben, and flupoxam. These may associate with several proteins involved with the process of cellulose synthesis (Sabba and Vaughn, 1999). Isoxaben is an extremely potent herbicide with an IC_{50} of 4.5 nM (Heim *et al.,* 1989). When grown in the presence of isoxaben, plants fail- to incorporate C^{14}-glucose into the insoluble fraction of *Arabidopsis thaliana* (see **Fig. 3)**, and grow isodiametrically due to the lack of mechanical strength to withstand internal turgor pressure (Heim *et al*., 1989; Sheible *et al.,* 2001). Heim *et al.* (1989) isolated two alleles, *CESA3*$^{ixr1\text{-}1}$G(998)D and *CESA3*$^{ixr1\text{-}2}$T(942)I*,* which confer extremely high resistance to isoxaben. *CESA6*$^{\text{Ixr 2-1}}$ R(1064)W was identified later by Desprez *et al.* (2002). Given the presence of independent alleles on separate proteins, it was suggested that CESA 3 and 6 maybe part of the same complex (Desprez *et al.,* 2002). Interestingly, isoxaben will compete for the binding site of CESA 3,6, 2 and 5 since knockouts in

CESA6$^{Ixr2\text{-}1}$ background enhance resistance (Desprez *et al.,* 2007). Flupoxam is another CBI that shows promise in the study of cellulose synthesis (see **Fig. 2.)**. Flupoxam is a highly halogenated triazole linked aromatic compound originally developed as a herbicide (see **Fig. 2.)** The effects of flupoxam are similar to that of isoxaben (Vaughn and Turley, 2001). In cultured cotton fibers, isoxaben and flupoxam produce spherical cell protrusions, detachments of the plasma membrane from the cell wall, increased pectin accumulation, wall thinning and reduced cell division along with incipient vacuole formation (Vaughn and Turley, 2001). Growing plants in the presence of flupoxam results in reduced cellulose incorporation, decreased root elongation and induction of a clubbed root phenotype often seen growing seedlings treated with microtubule inhibitory drugs such as oryzalin (Hoffman *et al.,* 1996; Hoffman and Vaughn, 1996). Interestingly, flupoxam does not destabilize microtubules like oryzalin (Hoffman and Vaughn, 1996). It was postulated that flupoxam may disrupt a similar mechanism but a separate binding site on the cellulose synthases, given that alleles resistant to isoxaben are sensitive to flupoxam (Vaughn and Turley, 2001).

2.4 Potential candidates to which the cellulose synthases may interact

There have been many mutations in a number of other proteins that certainly hinder the ability to produce cellulose but do not completely eliminate it (Somerville, 2006). The *KORRIGAN* (*KOR)* gene encodes a membrane β-1,4 glucanase which when knocked out exhibits reduced cellulose accumulation and altered pectin composition (Nicol *et al.,* 1998). It is plausible that *KORRIGAN* may have a role in removing non-crystalline glucan chains from the growing microfibril (Somerville, 2006). Another protein implicated in cellulose biosynthesis is COBRA (COB), a glycophosphatidylinositol (GPI)

anchored protein found in the cell wall (Roudier *et al*., 2005). Mutations in the *COB* gene leads to extremely dwarfed and cellulose deficient plants (Roudier *et al*., 2005). Mutations in the *CHITINASE LIKE 1 (CTL1) /POM1* gene result in reduced root cell expansion and decreased cellulose content (Hauser *et al.,* 1995). While the proteins mentioned all clearly contribute to some extent to cellulose synthesis, the contribution of other proteins is somewhat more tentative. For example, there is conflicting evidence whether Sucrose Synthase (SuSY) is associated with the cellulose synthases. Specifically, it has been shown that SuSY is a major component of the catalytic unit of the cellulose synthase complex (Fujii *et al.,* 2010). However, quadruple mutants of this gene result in no difference in cellulose content (Barratt *et al.,* 2001) indicated that it is a non-essential component. Another example is the recently discovered CELLULOSE SYNTHASE INTERACTING1 (CSI1), which has been shown to interact in a yeast two hybrid with the catalytic domain of both CESA1 and CESA6, but its functional importance has yet to be shown (Gu *et al.,* 2010). It was hypothesized that CSI1 may form a scaffold between CESA complexes, or mediate interaction with underlying microtubules (Gu *et al.,* 2010).

2.5 Cellulose synthase regulation at the protein level

Apart from these accessory proteins, no plant gene or small molecule responsible for the regulation of cellulose biosynthesis has been identified (Somerville, 2006). It is theoretically possible that there is some phosphatase or kinase regulating the activity of the cellulose synthases in plants (Somerville, 2006). Nuhse *et al.,* (2004) identified several phosphorylation sites in the CESAs particularly in the N-terminus through LC-MS/MS analysis of plasma membrane fractions. Furthermore, CESA turnover in secondary cell walls was shown to be the result of phosphorylation and targeted

proteolysis of CESA7 via the proteosome (Taylor, 2007). Recent work in which known phosphorylated serines were mutated to alanine or glutamate to either disrupt phosphorylation or promote phosphorylation show that anisotropic expansion is at least in part due to the modulation of CESA1 sites (Chen *et al.*, 2010). Similarly, Kaida *et al.*, (2009) showed that over expression of purple acid phosphatase activates membrane bound cellulose/callose synthases in tobacco cell culture. It has yet to be determined whether or not the purple acid phosphatase interacts directly with the cellulose synthase machinery or via an unknown intermediate (Kaida *et al.*, 2009).

2.6 Protein – protein interaction tools to study CESA interaction

Protein-protein interaction studies with potential CESA interactors are required in order to piece together the entire process of cellulose synthesis. Desprez *et al.*, 2007 demonstrated CESA-CESA interaction using BiMolecular Fluoresence (BIFC) complementation in tobacco leaves, but even with this method you cannot decipher whether or not additional proteins may be assisting in the interaction. Wang *et al*., 2008 synthesized specific primary antibodies to the N-terminal regions of cellulose synthase 1,3 and 6, and was successful in pulling down an intact 840 kDa complex that contained all three isoforms. However, the authors could not rule out the effect of additional proteins mediating the interaction between the primary cell wall CESAs. Timmer *et al*., 2009 demonstrated that a Membrane yeast-two hybrid MbyTH (Dual systems) approach could be used to characterize interactions between secondary cell wall cellulose synthases. One aspect discussed in this paper involves the development of a similar approach for use with cellulose synthases in the primary cell wall, specifically to look for interaction between CESA 1 and 3 without the effect of other endogenous plant proteins.

This approach is advantageous because it allows the use of full length CESA proteins. Many yeast two hybrid approaches using the CESAs have focused only on the soluble regions (Xu and Joshi., 2010; Gu *et al.,* 2010). This is because traditional Yeast 2 hybrid technology requires protein localization to the nucleus, and as such, proteins that go to the membrane cannot be studied (Bartel and Fields, 1995; Thaminy *et al.,* 2006). A membrane Yeast 2 hybrid (MbyTH) takes advantage of the nature of ubiquitin to study membrane interactions. Specifically, ubiquitin is split into two halves (Nub and Cub) which are attached to two proteins of interest (Bait and prey). Reconstitution of the two halves of ubiquitin results in cleavage by ubiquitin specific proteases and translocation of an attached transcripton factor to the nucleus. This bypasses the need for nucleus localization but still utilizes auxotrophic selection, the details to which are discussed in the methodology. It is predicted that interaction results should recapitulate previous *in-vivo* and *in-vitro* interaction studies (Desprez *et al.,* 2007; Wang *et al,* 2008).

2.7 Potential mechanisms of cellulose crystallization

Another aspect of the CESAs that has yet to be shown is how the cellulose synthases produce crystalline cellulose and whether or not the CESAs themselves are self-sufficient in this process. Plant cellulose can be found in two forms called cellulose Iα and Iβ, of which the latter is a triclinic symmetrical organization and the former being a monoclinic organization (Brown, 1996). Both forms are found in varying degrees of abundance between species (Brett, 2000). Nakashima *et al.* (2010) demonstrated that the tunicate chordate *Oikopleura dioca* developmentally controls whether it synthesizes Iα or Iβ cellulose. In plants, it is also not yet known the mechanism of glucan crystallization, and whether this is enzyme facilitated or the CESAs themselves are sufficient to do so

(Somerville, 2006). Jarvis (2000) suggested that crystallization may occur as the fiber bends out of the complex, the inner face of the fiber will slip to displace tensile stress and help position the chains for proper hydrogen bonding. Further, it is hypothesized that depending on the degree of bending in the membrane, the ratio of Iα:Iβ will be altered (Jarvis, 2000). The Iα:Iβ ratio could be altered by specifically modifying the molecular environment with which the microfibril bends (Jarvis, 2000). Interestingly, recent crystallization work of the GAxCesD protein in *Gluconoacetobacter xylinus,* show a spiral octomer that may help spin glucan chains together and assemble the crystalline structure (Hu *et al*., 2010). A similar mechanism may take place in plants in which some tensile stress on the fiber via position of the complex in the membrane may actually help the process. Harris *et al.* (2009) demonstrated that CESA amino acid subsitutions, specifically CESA$^{Ixr1\text{-}2}$ T(942)I which confer resistance to isoxaben (*IXR*), also alters the degree of cellulose crystallization, and this in turn leads to improved biochemical conversion to fermentable sugar. Given these findings, it seems plausible that genetic mutations chemically resistant to other cellulose biosynthesis inhibitors (CBIs) may also produce similar alleles to that of CESA3$^{Ixr1\text{-}2}$.

2.8 Genetic screens for flupoxam may identify further proteins involved in cellulose synthesis

Given that cellulose biosynthesis inhibitors (CBIs) disrupt cellulose synthesis through a means mediated by the protein machinery involved. We could use a genetic screen to isolate mutants resistant to a CBI; and hence, potentially isolate a new protein. More specifically, I wanted to test the hypothesis if the mode of action of flupoxam is similar to that of isoxaben and/or if flupoxam could be used to identify new players involved in

cellulose biosynthesis (Vaugn and Turley, 2001). In addition, I also wanted to test the nature of interactions between known cellulose synthase components using a membrane two hybrid system.

3.0 Methods

3.1 Plant material and growth conditions

All mutant *Arabidopsis* used were of the Landsberg (Ler) ecotype, except *fpx 1-1* which is of the Columbia (Col-O) ecotype. Seedlings were germinated and grown under continuous light (200 $\mu E/m^2/s$) or in the dark at 21°C on plates containing half-strength Murashige and Skoog (MS) mineral salts (Sigma-Aldrich, St. Louis, MO), 0.8% agar and supplemented with no more than 0.1% ethanol. Alternatively, plants were grown on a mixture of 70% sphagnum peat, 15% perlite and 15% vermiculite in chambers maintaining the following conditions: 21°C under long-day conditions (16 h light/8 h dark) at a light intensity of 200 $\mu E/m^2/s$. Flupoxam was a kind gift from Kureha Chemical Industry Co., Iwaki City, Japan. Seeds were obtained from the *Arabidopsis* Biological Resource Center at Ohio State University.

3.2 Forward genetics screen for flupoxam chemical resistance

45 000 seeds were treated with 0.3 % EMS (M1) for 16 hours at room temperature. They were then extensively washed with water over the course of 10 hours and sewn onto soil to generate the M2 seeds. One million M2 EMS treated seeds were surface sterilized and

screened for resistance on 20 nM flupoxam. Resistant mutants were isolated and transferred to MS. Plants were propagated and re-selected to confirm that the flupoxam resistance was heritable.

3.3 DNA purification using CTAB

Leaf tissue was ground in 150 µl of CTAB using a drillpress with a homogenizing bit in a sterile eppendorf tube. CTAB buffer consisted 100 mM Tris HCL pH 8.0, 1.4 M NaCl, 20 mM EDTA, and 2% w/v CTAB (cetyltrimethyl ammonium bromide). The homogenizing bit was then rinsed with another 150 µl of CTAB to clear left over tissue debris into the eppendorf tube. The tissue suspension was then incubated for one hour at 65°C. Following incubation, an equal volume of chloroform was added and the solution was vortexed and centrifuged for 10 minutes at 13,000 rpm. The aqueous phase was removed and an equal volume of 2-propanol was added to precipitate DNA, and the solution was vortexed and centrifuged for 10 minutes at 13,000 rpm. The DNA pellet was washed with 70% ethanol, air dried and dissolved in sterile H_20.

3.4 Next-generation mapping

fpx 2-2 and *fpx* 2-3 originally designated 45-1 and 43-1, respectively, were backcrossed to Columbia to generate an F2 mapping population. F2 seeds were selected on 20 nM flupoxam and grown to generate a pool of individuals all containing the mutant allele linked to the flupoxam resistance. Leaves from 50 individuals were pooled and ground

with a mortar and pestle in liquid nitrogen. DNA was extracted using the reagents and specifications of the Puregene DNA purification system (Qiagen; Valencia, CA). Purified DNA was sent to the University of Toronto for processing according to Next-generation mapping (NGM) protocols (Austin *et al*., 2011). Briefly, NGM takes advantage of a analysis used for Solexa/Illumina data processing; chastity belt statistic. The chastity-belt statistic measures the proportion of polymorphisms between the mutant and mapping parental lines and uses this to determine the regions in which there is exclusive segregation with the mutant parental line (Austin *et al*., 2011).

3.5 RNA isolation

RNA was extracted using an RNeasy Mini Kit (Qiagen; Valencia, CA). RNA was immediately used for first strand synthesis and excess RNA stored at –80C for further use.

3.6 First Strand Synthesis

One half to 2 μg of RNA was added to a sterile eppendorf tube along with 1 μl of 50 μM Oligo d(T) (NEB; Ispwich, MA), 1 μL of 60 μM Random primer (NEB; Ispwich, MA) and 4 μl of dNTP mix (2.5 mM each titrated with TRIS-Cl ph 7.0) (NEB; Ispwich, MA) . Mixture was heated for 5 min at 65°C and quickly placed on ice. 2 μL of reverse transcriptase 10x Buffer (NEB; Ispwich, MA) was added along with 1 μL 200,000 U/mL of M-MulV Reverse Transcriptase (NEB; Ispwich, MA) and 1 μL of 40,000 U/mL

RNase inhibitor (NEB; Ispwich, MA). The mixture was titrated to a final volume of 20 μL and incubated at 42°C for one hour. Reverse transcriptase was inactivated at 90°C for 10 min and products stored at -20C for later use.

3.7 Mutant Gene expression using qRT-PCR

Five milligrams of seeds were weighed out for each mutant plus a wild type control (n=3). Plants were transferred to six well plates containing 0.5x liquid MS (Sigma-Alrich; St.Louis, MO)/ 0.5% glucose and stratified for 4 days at 4°C. Plants were grown for 5 days at room temperature in the dark with gentle shaking. Tissue was ground in liquid nitrogen and then RNA was extracted using the RNeasy Mini Kit (Qiagen; Valencia, CA). Primers were designed using oligo-perfect to ensure all primers were 20 bp with a T_m of 60°C (http://tools.invitrogen.com/content.cfm?pageid=9716; Invitrogen; Carlsbad, CA). As well, amplicon size was standardized to around 100 bp for each of the experimental treatments and the ACTIN7 (At5g09810) control. cDNA was synthesized according to first strand synthesis protocol above and amplified with a C1000 thermal cycler CFX real-time system from Bio-Rad using iTaq SYBR Green Supermix (Bio-Rad; Hercules, CA), according to the manufacturers procedures. Optimal annealing conditions were determined as 55°C for *CESA*1 and *CESA*6 and 57.5°C for *CESA*3.

3.8 Gateway Cloning

cDNA obtained in first strand synthesis was amplified using Phusion High Fidelity DNA polymerase (NEB; Ispwich, MA) to obtain full length cDNA, according to the manufactures specifications. Amplified products were gel cleaned using the BioBasic gel extraction kit (Biobasic; Markham, ON). Products were then cloned into pENTR/D-TOPO (Invitrogen; Carlsbad, CA) using the enzyme topoisomerase (Invitrogen; Carlsbad, CA) which directionally clones PCR products containing a 5' CACC recognition sequence included in the **Table. 2** into the pENTR vector (**Fig. 25.**). Reaction conditions were according to the manufacturer's specifications. Cloning reactions were transformed into DH5 alpha Max efficiency cells (Invitrogen; Carlsbad, CA), according to manufacture recommendations. All plasmids were subjected to both restriction enzyme digestion and sequencing to verify the validity of the clone. DNA sequencing was accomplished by capillary-based fluorescent sequencing on dual ABI 3730XL instrument at the Sick Kids TCAG DNA sequencing facility using the primers M13 forward and M13 Reverse for verification.

3.9 Restriction enzyme cloning in MbyTH plasmids

cDNA was amplified from pENTR/D-TOPO clones previously isolated. A list of primers is provided in **Table 5**. Cloning into MbyTH vectors was accomplished using SfiI overhangs with some exceptions. The stop codon was removed for all plasmids containing a C-terminal fusion and replaced with an in frame glycine (pBT3STE (**Fig. 26.)**, pPRESTE (**Fig. 29.)**). For pPRESTE (**Fig. 29.)**, a leucine was added to maintain frame with the upstream SteII leader sequence. For all amplifications with *CESA*1, a

glycine linker was added to the 5' sequence to prevent formation of a secondary SfiI cut site. SfiI overhangs were added for pBT3N (**Fig. 31.**) and pPR3N (**Fig. 32.)**. Amplified products were gel cleaned using the BioBasic Gel extraction kit. Amplified products were subject to restriction enzyme digestion with SfiI (NEB; Ispwich, MA) and ligated using using T4 DNA Ligase (NEB; Ispwich, MA) according to Sambrook and Russel, (2001). At least three replicates of each clone were sent for plasmid sequencing. DNA sequencing primers can be found in **Table 4.**

3.10 Midiprep plasmid isolation using the alkaline lysis method

All reagents here were made according to Appendix 1 of the Molecular cloning manual (Sambrook and Russel, 2001). Transformed colonies were inoculated into 5 mL of Luria-Bertani (LB) broth with 100 μg/mL ampicillan (Bioshop; Burlington, ON) or 50 μg/mL kanamycin (Bioshop; Burlington, ON) and incubated overnight in a 15 mL falcon tube at 220 rpm and 37 degrees. Following this, 200 μl of cold alkaline lysis solution I was used to resuspend the pellet and transferred to a microcentrifuge tube. The tubes were then vortexed vigorously and 400 μl of fresh alkaline lysis II was added to the bacterial suspension and inverted approximately 5-10 times. 300 μl of alkaline lysis solution III was then added, inverted 5 times and stored on ice for 5 minutes. The solution was centrifuged at 13,000 rpm for 5 minutes and 600 μl of supernatent transferred to a new tube. An equal volume of phenol:chloroform was added and supernatent again transferred to a new tube. Plasmid DNA was precipitated with an equal volume of 2-propanol and centrifuged at maximum speed for 10 minutes. Plasmid pellets were washed with 70% ethanol, dried and dissolved in 100 μl of sterile H_20. Five microgram of RNase was added to all plasmid solutions and subject to 50°C for one hour.

3.11 Processing tissue material

All plants were harvested at maturity, at the same time and under the same conditions. Dry, senesced plant tissue desiccated in a 60°C oven for 24 hours. Plants were ground using a Wiley mill fitted with a 1mm screen. All replicates represent a pool of 6 individual plants. The tissue was then subject to a washing protocol. To do this, 10 mL of water was added to the tissue and shaken gently at room temperature until the tissue was saturated. Tissue was then subject to an additional water wash at 80°C. Following aspiration, 10 mL of 70% ethanol was added and incubated again at 80°C. Lastly, 10 mL acetone was added and incubated at room temperature for one hour. Acetone was removed and tissue was then allowed to dry for 2 days at room temperature.

3.12 Determination of cellulose crystallinity

Dried and processed senesced material was loaded onto an aluminum sample holder with a glass background, into a PANalytical Phillips PW3170 X-ray diffractor at the Department of Geology, University of Toronto. Material was pressed by hand using a scuptula to generate an even surface. Protocols were run with start angle of $2\theta = 4.5°$ and an end angle of 30°. The scan speed was run at 0.008 °2θ/s, an intensity of 40kV and 40 mA. Data was calculated using the equation for Relative crystallinity index (RCI) used by Segal *et al*., (1959) where $RCI=I_{002}-I_{am}/I_{002} \times 100$. I_{002} is the maximal peak around 21.5-22.5 representing the pure crystalline fraction as compared to an Avicel-cellulose control (Sigma-Alrich; St.Louis, MO). The I_{am} is the trough found around 2θ 18-20°, this is a due to amorphous scattering (Segal *et al.,* 1959). An average of 10 peaks was taken at the

amorphous trough and the crystalline peak areas. Results indicated are a product of n=3, with each replicate containing plant material pooled from 6 plants.

3.13 *In vivo* C^{14}-glucose incorporation studies

Five milligrams of homozygous seeds were weighed out on a microbalance Mettler Toledo AB204-S scale. Seeds were surface sterilized in a chlorine gas chamber and transferred to six well plates containing 5 mL of 0.5x liquid MS (Sigma-Alrich; St.Louis, MO)/ 0.5% glucose. Seeds were then stratified at 4°C for 3-4 days. After this, plants were grown on an orbital shaker in the dark at medium speed. After five days of growth, seedlings were washed three times in 5 mL glucose free medium and resuspended in 2 mL of 0.5x MS containing 0.5 μCi/mL C^{14}-glucose (American Radiolabelled chemicals; St-Louis, MO). Seedlings were then incubated for 1 hour in the dark on an orbital shaker. Following treatment, seedlings were washed three times with 5 mL glucose free medium. These were then transferred to glass tubes and incubated in 5 mL ethanol in a 80°C waterbath for 20 min. This was repeated three times. Seedlings were then incubated in 3 mL chloroform:methanol (1:1) for 20 min in a 45°C water bath. Finally, seedlings were incubated in 5 mL of acetone at room temperature for 15 min. The acetone was aspirated and the tissue was allowed to dry for two days before being weighed. Material was then treated according to Updegraff (1969) with minor modifications. One mL of updegraff solution (Nitric acid: Acetic acid: water 1:8:2) was used to hydrolyze the cell wall material by incubation in a boiling water bath for one hour. Soluble and insoluble fractions were separated using a 12 well suction filtration system. The insoluble fractions were retained on Watman 25 mm GF/A glass microfilters and tubes washed one time with 1 mL water. The flow through and 1 mL water wash represented the soluble

fraction. Both soluble and insoluble fractions were transferred to scintillation vials, and 5 mL of Ultima gold high flash point scintillation liquid cocktail (Perkin Elmer; Waltham, MA) was added. Vials were counted using a Perkin Elmer Tri-carb 2800 liquid scintillation detector (Waltham, MA). Data was either expressed as raw counts per minute (cpm) of insoluble fraction (**Fig. 3.)** or as a percent incorporation ([insoluble/(insoluble + Soluble)]*100) (**Fig. 12.**). Data presented in **Fig. 12** is the combination of 5 separate experiments with varying replications over the course of one year.

3.14 Reducing sugar determination via the anthrone photometric method

Five mg of washed tissue (n=6) was carefully weighed using a Mettler Toledo AB204-S microbalance and placed in eppendorf tubes. Tissue was macerated in 800 μl of water for 1 hour on an orbital shaker. Following thorough hydration, 200 μl of 1M H_2SO_4 was added to each sample and the mixture was vortexed and incubated at 50°C for 5 hours. At the first hour, solutions were removed from the waterbath, centrifuged at 13,000 rpm for 10 minutes and 50 μl of sample was removed and added to a 96 well plate. 50 μl of water was added to each sample to return the total volume to 1 mL, and samples returned to the 50°C waterbath. While samples incubated, one hour samples were processed using anthrone photometric method. A multichannel pipette was used to add 100 μl of cold 0.2% anthrone (Sigma-Alrich; St.Louis, MO) in concentrated H_2SO_4. The solutions were mixed by pipetting repeatedly 10 times to ensure thorough reaction completion. The 96 well plate was then incubated on a 100°C heat block for 5 minutes and cooled at 4°C for

5 minutes. Absorbance was read at A_{620} nM using a Bio-Rad xMark microplate spectrophotometer (Hercules, CA) and absorbance was correlated according to standard glucose curve (**Fig. 19.**) This procedure was repeated each hour for 5 hours.

3.15 Scanning Electron Microscropy

Five day old seedlings were first immersed for 30 seconds in pure anhydrous methanol. They were then fixed for 24 hours in FAA (50% ethanol, 5% acetic acid, 3.7% formaldehyde). After this incubation, the tissue was dehydrated in an ethanol series (+5%/hour) and stored in 100% ethanol for 24 hours prior to being critically point dried using Autosamdri-815 drier and gold sputter coated using a Balzer Sputtering device. Samples were visualized using a Hitachi S2300 scanning electron microscope at the Department of Cell and Systems Biology, University of Toronto.

3.16 Light Microscopy

Light microscope pictures were taken using an AmScope dissecting microscope and visualized using an Amscope MD900E camera (Irvine, CA).

3.17 Plasmid maintenance

Plasmids were propagated in chemically competent E.Coli (NEB #C2925) and transformations carried out according to Sambrook and Russell (2001).

3.18 Yeast Plates

All media plates were made according Finley and Brent (1995), using reagents from Bioshop (Burlington, ON).

3.19 Membrane Yeast two hybrid

Yeast two hybrid was carried out according to protocols provided by Dualsystems Biotech AG, Zurich Switzerland with modification using the NMY 51 yeast strain (MATa his3delta200 trp1-901 leu2-3,112 ade2 LYS2::(lexAop)4-HIS3 ura3::(lexAop)8-lacZ (lexAop)8-ADE2 GAL4). This two hybrid system exploits the modular features of ubiquitin proteosome pathway. Briefly, ubiquitin is separated into its two halves Cub and Nub, which are cloned in frame with a "bait" and "prey", respectively. Attached to Cub is the transcriptional binding domain of bacterial LexA and the transactivator VP16. Upon reconstitution of the two halves of the ubiquitin, cleavage of ubiquitin by ubiqtuitin specific proteases results in release and translocation of the transcriptional activator to the nucleus. Plasmid maintenance is accomplished by selection on medium lacking leucine and tryptophan, since presence of the plasmid code for *LEU* and *TRP1* genes **(Fig. 26., Fig. 29.)**. Further, protein constructs which strongly interact result in the cleavage of LexA-VP16, binding to LexA operators and activation of *ADE2* and *HIS3* genes, growth on media lacking adenine and histidine, respectively. Also, the inability to transcribe the *ADE*2 gene, results in the accumulation of a red intermediate. Also, LexA-VP16 will initiate transcription of LacZ β-galactosidase, which cleaves substituted galactose compounds such as Xgal (bromo-chloro-indolyl-galactopyranoside) (Bioshop;

Burlington, ON)**.** It is important to note that ubiquitin will not reconstitute unless the two halves are attached to proteins which come into close proximity. This is due to a mutation in the Nub half of ubiqituitin from an isoleucine (NubI) to glycine (NubG). This mutation completely abolishes reconstitution, successful reconstitution only occurs if fused to an interacting pair of proteins. Any protein of interest fused to Cub if translated successfully and folded properly will exhibit strong interaction with NubI but not with nonspecific proteins fused to NubG. Therefore, these can be used as a functional test in the MbyTH. Specifically, if a functional protein is translated, there will be strong interaction with the test protein pOST1NubI but not pFe65NubG. Constructs were cloned as described previously and summarized in **Table 1**. Transformation into yeast was performed using a standard polyethylene glycol (PEG)/lithium acetate protocol (Gietz and Woods, 2001). The host strain, NMY 51 was grown in a 50 mL liquid YPAD (yeast extract-peptone-adenine-dextrose) overnight to an OD 0.6-0.8 in a 30°C incubator at 145 rpm. In order to rule out any complications with plasmid functionality, three *E. Coli* independent plasmid clones for each construct were pooled and used for each transformation into the yeast strain. Bait and prey (**Table 1.**) were Co-transformed using the PEG/LiOac method (Gietz and Woods, 2001)**.** Approximately 500 transformants were re-streaked, allowed to grow and re-inoculated into standard dropout media lacking tryptophan and leucine overnight. One milliliter of 1.0 x 10^8 cells (OD 0.4) was used for subsequent experiments. Cells were diluted 0x, 10x, 100x, 1000x and plated using a multichannel pipette on media lacking tryptophan, leucine to maintain the plasmids as well as histidine and adenine to test the strength of interaction. Functionality of the construct was tested by activation with the positive control constitutive pOST1 -NubI (**Fig. 28**) mutant, and the absence of

self activation confirmed by lack of interaction with the negative control pFe65-NubG (**Fig. 27.**). Strong interactions were assayed supplemented with dropout media + 10 mM 3-amino-1,2,4-triazole(3AT) (Bioshop; Burlington, ON), which is a competitive inhibitor of the *HIS*3 gene. Only when there is a strong interaction between two proteins can the yeast grow in the presence of 3AT, since strong expression of *HIS3 is* needed to overcome the *HIS*3 inhibition.

3.20 Transmembrane Modelling

Protein sequences for CESA 1 and CESA 3 were diagramed using the Residue based Diagram editor (RbDe) at http://icb.med.cornell.edu/crt/RbDe/RbDe.html. (Campagne and Weinstein, 2000). The algorithm and diagram layout was also designed and implemented by Campagne and Weistein, (1999).

3.21 Sequencing alignment

Sequencing alignment and plasmid construction was conducted using CLC DNA workbench (CLC Bio, Denmark).

3.22 Statistical Analysis

A one way analysis of Variance or paired T-Test was performed using SigmaPlot (San Jose, CA) in which the null hypothesis was rejected above the p=0.05 level. Chi-Squared values were calculated by hand and p values determined using a critical values of chi-square distribution chart (Samuels and Witmer, 2003).

4.0 Results

4.1 Flupoxam is a Cellulose Biosynthesis Inhibitor

Flupoxam displays characteristics of a cellulose biosynthesis inhibitor (CBI). Landsberg plants grown in the presence of 5 nM flupoxam display blebbing cell structure particularly noticeable on the epidermis of cotyledons (**Fig. 1.)**. Landsberg plants grown for 5 days prior to being incubated in C^{14} –glucose + 1 μM flupoxam displayed reduced incorporation into the insoluble cellulosic fraction following Updegraff treatment, in comparison to C^{14} –glucose incorporation in the absence of flupoxam **(Fig. 3.)**. Also, flupoxam disrupted C^{14} –glucose incorporation into the cellulosic fraction at a similar level to that of seedlings incorporating C^{14} –glucose in the presence of isoxaben (**Fig. 3.)**.

4.2 Novel Genetic Mutations Exhibit a Range of Resistance to Flupoxam

A chemical screen was performed on 1, 000,000 M2 seeds, 31 putative mutants were grown to adulthood (M3 population) and retested on flupoxam. Of these 31, 25 plants exhibited heritable flupoxam resistance. Of the M3 population, all flupoxam alleles were non-segregating, meaning the mutant screen had only isolated homozygous alleles which could be recessive or dominant. In order to determine inheritance, lines have to be backcrossed and re-selected on flupoxam. A summary of the putative mutants and identified mutant alleles can be found in **Table 6.** To further characterize putative mutations we endeavored to positionally clone the potential genes. For some of the alleles that were isolated this was accomplished using NGM techniques (Austin *et al*., 2011).

NGM revealed three novel mutations (*fpx 2-2, fpx 2-3, fpx 2-4)* in the long arm of chromosome 4 in the gene *CESA* 1 (At4G32410). The mutations all cause single amino acid substitutions *fpx 2*-2 leads to a P(1010)L, *fpx 2-3* leads to a G(1009)D, and *fpx 2-4* a S(307)L (**Fig. 7., Fig. 34.).** *Fpx 2-4* S(307)L is discussed in the appendix. Given the evidence of mutations in *CESA1*, sequencing of the C-terminal ends of *CESA1* and *CESA3* (At5G05170) in the remaining putative mutants revealed 4 more novel mutations. Sequencing using primers from **Table 4.**, revealed novel mutations corresponding to *fpx* 2-1 G(1013)R on *CESA* 1, as well as *fpx* 1-1 S(1040)K, *fpx* 1-2 S(1037)F, and *fpx* 1-3 S(983)F on CesA 3. The DNA chromatograms are shown in **Fig. 6.** and **Fig. 7..** Also, their relative amino acid position of the substitutions (**Fig. 8.)**. *fpx* 2-1, *fpx* 2-3, and *fpx* 1-2 have the greatest relative resistance, while *fpx* 1-1, *fpx* 1-3, and *fpx* 2-2 are less resistant to flupoxam (**Fig. 4..)**. Although there are clear differences between mutants at the level of resistance to the herbicide (**Fig.4.)**, mature plants did not display any dwarfism in comparison to controls (**Fig. 9.** and **Fig. 10.)**.

4.3 In-Vivo cellulose incorporation

Given the relative importance of *CESA1* and 3 in the enzymatic catalysis of β1-4 glucan, we wanted to test whether or not levels of *in-vivo* cellulose incorporation was at all affected. The level of C^{14} –glucose incorporation was assessed for each mutant and expressed as a percent of incorporation into the cellulosic fraction (%incorporation = (insoluble/(soluble + insoluble))*100. Only *fpx* 2-1 showed a small, albeit significant decrease in cellulose incorporation according to a Dunnett one-way anova (n=16, p=<0.001) (**Fig. 11.)**. There was no significant difference between Ler (n=28) and

Columbia (n=20) (p=0.088) (**Fig. 11.)**. Mutants *fpx* 1-1 (n=22), *fpx* 1-2(n=18), *fpx* 1-3(n=17), *fpx* 2-2 (n=20), and *fpx* 2-3(n=16) did not show significant decreases in % cellulose incorporation relative to control according to a Dunnett one-way anova in comparison to controls (p=0. 530, p=0.234, p=0.181, p=0.421, 0.997) (**Fig. 11.).**

4.4 Determination of Cellulose Crystallinity

Since the *fpx* mutations did not have any effect on the catabolic activity of the enzymes, we reasoned that the mutations may have alterations in the crystalline nature of cellulose. An X-ray diffraction method was pursued to test this hypothesis. Briefly, a pure crystalline material such as pure cellulose will deflect an incident x-ray beam at a specific angle of symmetry. Looking at a diffraction diagram of pure cellulose in **Fig. 12.**, a crystalline peak is observed at a diffraction angle of 22.5° 2θ The relative crystallinity index (RCI) of tissue was calculated according to standard method as discussed in the methodology. Replicates shown in **Fig. 14.** are the combination of triplicate runs containing the pooled tissue from 6 individual plants. Wild type crystallinity measured around 48.4% for landsberg and 49.2% for Col-O, the difference of which is not significant according to a dunnett one way anova ($p>0.05$). Certain mutations on *CESA*1, *fpx* 2-1, *fpx* 2-2 and *fpx* 2-3 show a significant 20% decrease in relative crystallinity ($p<0.05$)(**Fig. 14.)**. The diffraction pattern for these mutants are shown in **Fig. 13.** All other mutants tested do no show significant changes in RCI in comparison to wild type (**Fig. 14.)**.

4.5 Biochemical conversion of mutant biomass to reducing sugar equivalents

Given the changes in the x-ray diffraction patterns of the various *fpx* mutations, it was hypothesized that changes in crystalline cellulose would improve acid digestion into fermentable sugar. This is because increases in interchain spacing should correlate to increases in surface area and hence improve acid catalyzed cleavage of glycosidic linkages. An anthrone photometric method was undertaken to look for changes in reducing sugar release. They were compared to standard glucose controls as a measure of relative glucose equivalents released over the course of 5 hours. Exposure of dried senesced tissue to acid hydrolysis resulted in significant increases in sugar release over time with *CESA*1 mutants *fpx* 2-1 *fpx* 2-2 and *fpx* 2-3 according to a Dunnett one way anova ($n=6$, $p<0.05$)(**Fig. 20.)**. Acid hydrolysis of *CESA*3 mutant tissue resulted in significant increases glucose equivalents released by *fpx* 1-2 and *fpx* 1-3 ($n=6$, $p<0.05$)**(Fig. 19.)**, whilst *fpx* 1-1 exhibited significant decreases in release of glucose equivalents compared to a Columbia control ($n=6$, $p<0.05$)**(Fig. 18.)**.

4.6 Mutant *fpx* cellulose synthase expression profile

There is evidence that the CESAs are phosphorylated for anisotropic expansion, turnover, and that they are potentially regulated through a phosphatase or kinase (Nuhse *et al.*, 2004; Chen *et al.*, 2010; Somerville, 2006). Given that cellulose biosynthesis is probably a tightly regulated process, any defect involving regulation at the protein level may reverberate at the expression level. For example, it was hypothesized that if turnover was stagnant, expression levels would wane as the plant cell reaches equilibrium between

cellulose deposition and growth. The variation in *CESA1*,*CESA3* and *CESA6* transcript was assessed using qRT-PCR (**Fig. 15., Fig. 16., Fig. 17.)**. The mutants do not display drastic changes in *CESA3* and *CESA6* transcript. However, it seems there is fluctuation in *CESA1* expression amongst the mutants. Most notably, *CESA1* expression is altered in *fpx* 1-2, *fpx* 2-1, and *fpx* 2-3.

4.7 Membrane Yeast two Hybrid (MbyTH)

A membrane yeast two hybrid (Y2H) seemed like a reasonable method that could be employed to study CESA interactions. In contrast to traditional Y2H, a membrane yeast two hybrid (MbyTH) would allow full length membrane protein interaction to be examined. Specifically, we wanted to test the efficacy of using MbyTH on the CESAs and hopefully be able to use this approach to search for additional interactors, as well as characterize changes in CESA-CESA interaction with mutant alleles. Further, it could also be used to determine if cellulose biosynthesis inhibitors disrupt protein interactions at the membrane. Recombinant CESA1 and CESA3 were assessed for functionality in the MbyTH with Cub-lexA-VP16 either on the C-terminus or N –terminus (**Fig. 21.)**. pOST1 - NubI is used to assess the relative strength of interaction since constitutive interaction will occur only in the presence of stable proteins (**Fig. 28)**. It was determined that C-Terminal fusions are more functional based on strong interaction on standard dropout media –TLH + 10 3AT as well as –THLA (**Fig. 21.)**. C-Terminal fusions of CESA1-Cub-LexA-VP16 (CESA1 pBT3STE) tested against a C-terminally fused Cesa 1 –HA-NubG (CESA1 pPRESTE) grew strongly in –TLH/-TLHA with 10 mM-3AT but did not grow

when tested with any other prey (**Fig. 22.)**. Yeast containing the control plasmids pTSU2APP and pFe65-NubG showed strong growth as predicted(**Fig. 22.)** (Bresler *et al*., 1996). In addition, yeast carrying pFe65-NubG did not grow when co-transformed with CESA1 pBT3STE indicating interaction with this bait is not non-specific (**Fig. 22.)**. CESA1 pBT3STE interacted strongly with the positive control pOST1NubI indicating CESA1 pBT3STE is most likely functional (**Fig. 22.)**. C terminally fused CESA3-Cub-LexA-VP16 (CESA3 pBT3STE) did not interact nonspecifically with pFe65NubG and is functional based on strong interaction with pOST1NubI (**Fig. 23.)**. CESA3 pBT3STE exhibits strong interaction with all CESA3 constructs even when *fpx* alleles are present (**Fig. 23.)**. LacZ expression determined through the cleaveage of X-Gal is not as prominent as the positive control but still noticeable (**Fig. 22., Fig. 23.).**

CESA 1 and 3 combinations with C-terminal fusions were then assessed interaction with N-terminally fused preys of the same protein (**Fig. 24.)**. When CESA1 pBTESTE was tested against an N-terminally fused CESA1 pPR3N (**Fig. 24.)**, the result was the same as shown previously with CesA1 pPRESTE (**Fig. 22.)**. There was also strong interaction with CESA 3 pBT3STE was transformed along with N-terminally fused CESA 3 pPR3N (**Fig. 24.)**. When the prey protein has an N-terminal fusion (pPR3N) as opposed to C-terminal Fusions (pPRESTE) the interaction between CESA1 and CESA3 is stronger (**Fig. 24.)** then with C-terminal fusions (**Fig. 22., Fig. 23.).** This suggests a C-terminal fusion may be disrupting the inter-CESA interaction between CESA 1 and 3.

5.0 Discussion

Plant cellulose synthases are a group of enzymes that form a large multimeric cellulose synthase complex on the membrane surface (Crowell *et al*., 2009). This higher order complexity in the membrane as well as the inability for biochemists to purify and track activity enzymatically, has resulted in slow and cumbersome field of research. Despite many obstacles, there have been significant advances (Somerville., 2006). Many approaches have been used to begin to piece together this process. These include the study of targeted knockouts to discern the relative importance of the 10 CesA genes in *Arabidopsis* (Turner and Somerville, 1997; Desprez *et al.,* 2007; Richmond, 2000). The use of molecular fluorescence techniques to track the movement of CesA particles and how they move and distribute amongst a plant cell (Crowell *et al*., 2009; Desprez *et al.,* 2007) Mutagenesis studies have revealed numerous mutations on a wide range of proteins believed to be involved in cellulose synthesis (Somerville, 2006). We decided to employ a chemical genetics approach using the chemical herbicide flupoxam. Flupoxam causes many similar effects to isoxaben including the spherical protrusion of cells as a result of reduced cellulose synthesis, detachments of the plasma membrane from the cell wall, increased pectin accumulation, wall thinning, reduced cell division along with incipient vacuole formation (Vaughn and Turley, 2001). Genetic evidence for the mode of action of isoxaben is identified on CESA3$^{Ixr1\text{-}1}$ G(998)D; CESA3$^{Ixr\ 1\text{-}2}$ T(942)I) and CesA 6 *Ixr* 2-1 R(1064)W (Heim *et al*., 1989; Desprez *et al.,* 2002; Vaughn and Turley 2001). Given that they are sensitive to flupoxam, it seemed plausible that flupoxam may disrupt the CESAs on a separate binding site (Vaughn and Turley, 2001) Surprisingly, a screen of 1 million EMS treated seeds on 20 nM allowed us to isolate six new mutations on *CESA1*

and *CESA3*. It is interesting to note, CESA1$^{fpx\ 2\text{-}1}$ G(1013)R is in the exact same position as CESA3$^{Ixr\ 1\text{-}1}$ G(998)D discovered by Heim *et al. (*1989), both exhibiting no cross resistance to isoxaben or flupoxam. The mutations discussed in this study show varying degrees of relative resistance to flupoxam **(Fig. 4.)** At least on CESA1, the change in polarity may be more important than the change in charge given that the change of a Pro to Leu (both hydrophobic) in *fpx* 2-2 is not as chemically resistant as those of polar subsitutions in *fpx* 2-1 (Gly to Arg) and *fpx* 2-3 (Gly to Asp)(**Fig. 9.)**. All amino acid substitutions on CESA3 are hydrophobic serine substitutions to Phenylalanine (*fpx* 1-2 and *fpx* 1-3) and Leucine (*fpx* 1-1) (**Fig. 8)**. Further, resistance is favored by amino acid substitutions that are predicted to be at the cytosol-membrane border (**Fig. 9)**. Flupoxam itself has both a relatively nonpolar aromatic triazole group and a highly halogenated aliphatic side chain (**Fig. 2.)**. Given the nature of the molecule and the non-polar substitutions, it was hypothesized that flupoxam occupies both a membrane-cytosolic interface between CESA 1 and 3. This interface is predicted to occur in the last transmembrane region of CESA 3, representing the two adjacent serines in the last alpha helix (**Fig. 8)**. The halogenated side chain of flupoxam may disrupt potential hydrogen bonding between these serines and some undetermined protein, or CESA1 itself (**Fig. 8.)**. The potentiality for a role of serines in phosphorylation through a means that is mediated by CESA1 is less probable, given that phosphoproteomic studies did not identify these sites as phosphorylated (Nuhse *et al.,* 2004)**.** For now, we may pursue the approach that flupoxam disrupts a region shared by both CESAs and that flupoxam disrupts this interaction. Using the membrane yeast two hybrid (MbyTH) approach used in this study, interactions exhibited between CESA1/CESA1 and CESA3/CESA3 were tested for X-

Gal cleavage in the presence of 1 uM flupoxam. However, the effect of flupoxam on these interaction cannot be judged using LacZ expression alone given the weakness of blue coloration on X-Gal containing media.

In order to determine the effect of these mutations on enzymatic synthesis of β-1,4-glucan, an *in vivo* C^{14}-glucose approach was pursued. Even through many replications, only *fpx 2-1* exhibited a small albeit significant decrease in the incorporation of radiolabelled glucose into the insoluble fraction ($p<0.05$) **(Fig. 11.)**. Further, *fpx* mutants do not display indications of dwarfism as indicated by normal stature as adults **(Fig. 9.** and **Fig. 10.)**. Since mutations did not display drastic reduction in enzymatic glucose incorporation in cellulose, it was hypothesized that some other aspect of the cellulose synthase must be perturbed. To this end, we assessed the mutant dry biomass for alterations in cellulose crystallinity. Given that previous findings have found CESA3$^{Ixr\ 1\text{-}2}$ T(942)I not only has reduced crystallinity but also enhanced fermentable sugar release, it seemed reasonable that mutations identified here should have a similar effect to the cell wall. Relative crystallinity was standardized using a pure cellulose control and the relative crystallinity index (RCI) determined (**Fig. 12.)**. RCI values for wild type agree with previous findings of whole plant ranging from a 47-50% RCI (Harris and Debolt, 2008). All mutations on CESA1$^{Fpx\ 2\text{-}1,\ Fpx\ 2\text{-}2,\ Fpx\ 2\text{-}3}$ along with CESA3$^{Fpx\ 1\text{-}2}$ indicate a 20% and 10% drop in crystalline cellulose, respectively (**Fig. 14.)** Looking at the X-ray diffractograms in **Fig. 13.,** some mutants have relatively large increases in the amorphous scattering zone around 18° 2θ, as well as decreases in the crystalline peak around 22.5°θ. Using the anthrone photometric method as a crude assessment of total sugar release, it was determined that *CESA*1$^{\text{Fpx 2-1, Fpx 2-2, Fpx 2-}}$

^{3}mutations (**Fig. 20.)** are more susceptible to acid hydrolysis than mutations on CesA3$^{Fpx\ 1\text{-}2,\ Fpx\ 1\text{-}3}$ (**Fig. 19.)** *CESA3*$^{Fpx\ 1\text{-}1}$ produced decreased susceptibility to acid hydolysis, while this is strange, it may be just a result of increased Columbia wild type sugar release (**Fig. 18.)**. While the changes in crystallinity and the effect on sugar release is hard to interpret with this data alone, Harris *et al*. (2009) hypothesized that amino acid changes close to site of cellulose extrusion may modify the angles required for proper cellulose crystallization. Based on the model proposed by Jarvis (2000), crystallization of glucan chains may occur as the fiber bends out of the complex, the inner face of the chain will slip in order to relieve tensile stress. Given the nature of the mutations on CESA1$^{Fpx\ 2\text{-}1,\ Fpx\ 2\text{-}2,\ Fpx\ 2\text{-}3}$ where glycine, proline and glycine are replaced by arginine, leucine, aspartic acid, and that they are found at the bottom of an alpha helix, it is plausible that this region when mutated changes the bend of the alpha helix and therefore relieves some stress on the CESA complex required for crystalline cellulose (**Fig., 8).** Furthermore, less stress may have partial effect on the crystallization of the glucan chain through incomplete inter and intrachain hydrogen bonding. Furthermore, the isoforms of cellulose Iα and Iβ have been shown to contain different profiles of inter and intrachain hydrogen bonding, with Iβ being the more stable of the two due to more interchain bonding (Nishiyama *et al*., 2002/2003). Given that even between species the proportion of Iα can differ substantially between species (Brett, 2000), it must be possible that inter-intrachain hydrogren bonding can be tailored genetically. Certainly, evidence has shown the tunicate chordate *Oikopleura dioca* can control developmentally whether it synthesizes Iα or Iβ cellulose (Nakashima *et al.,* 2010). Therefore, it seems possible that the genetic mutations discussed here resulting in decreased crystallinity may be the result of differences in

inter-intrachain hydrogen bonding due to altered glucan slippage. In order to fully understand the nature of the chain dimensions, synchrotron x-ray diffraction and neutron diffraction similar to Nishiyama *et al*., 2002 must be undertaken to determine the extent of hydrogen bonding disruption.

Expression analysis of primary *CESA* genes in the mutants was assessed to look for alterations in *CESA* expression as a result of some perturbed effect of *fpx* alleles. While there seems to be fluctuations in *CESA1* transcript as determined by qRT-PCR, these cannot be correlated with any other phenotype described in this study. Given the importance of *CESA1* in cellulose biosynthesis, alterations in expression could potentially be a homeostatic response to cell wall defects.

One of the aspects of this project was the utilization of a membrane yeast two hybrid approach to delineate interactions with the cellulose synthases (Stagljar *et al*., 1998). The downside to traditional yeast two hybrids is that interaction is targeted to the nucleus (Bartel and Fields, 1995). The split ubiquitin method occurs on the membrane and therefore can accommodate membrane proteins (Stagljar *et al.,* 1998). Many yeast two hybrid approaches to study CESA interactions are forced to only study interaction with soluble regions of these proteins (Xu and Joshi., 2010; Gu *et al*., 2010). A membrane yeast two hybrid approach will allow the study of full length primary cell wall CESAs. A similar approach has been used for secondary cell wall CESAs (Timmer *et al.,* 2009). N-terminal fusions with the CESAs were shown to be less functional as demonstrated by interaction with NubI in comparison to C-terminal fusions (**Fig. 23).** It is interesting that Timmer *et al*., 2009 conducted their entire experiments with N-terminal fusions, but one cannot rule out difference between the primary and secondary cell wall

CESAs. A screen was conducted in which C terminal fusions of CESA1/CESA3 pBT3STE was paired against all potential cloned interactors (**Fig. 22., Fig. 23., Table 1**). It was found that CESA1 interacted strongly with itself but with no other prey (**Fig. 22.**). CESA3 was shown to interact strongly with itself as well, even with the CESA3 replications containing the amino acid substitutions (**Fig. 23.**). Interactions with CESA3 and the mutant CESA3 was only assessed qualitatively so any small change in interaction was not quantified. A more qualitative assay is required such as the ONPG assay (Miller, 1972). There was also a slight interaction observed between POM1 and CESA3. POM1 or CTL1 is a chitinase like protein despite not having any chitinase enzymatic activity in vitro (Hermans et al., 2010). Mutants in CTL1 show increased radial swelling in the root and decreased cell elongation. Interestingly, POM1/CTL has been shown to phenocopy CESA3 and CESA6 in response to environmental stress, and lignin deposition (Hermans et al., 2010). The interaction between POM1 and CESA3 in this MbyTH needs to be further pursued. Given the fact many others have show strong interactions between CESA1 and 3, it seemed troubling that similar interactions were not shown here (Desperez *et al.,* 2007 and Wang and Elliot 2008). Based on this, it was proposed that the C-terminally fused CESAs may hinder interaction between CESA1 and CESA3. Therefore, we decided to examine whether the interaction between CESA 1/3 could be reconstituted using preys with N-terminal fusions. Interaction between CESA 1 pBT3STE interacted strongly again with CESA1 pPRESTE, as well as CESA1 pPR3N N-terminal fusions (**Fig. 24.)**. CESA3 pBT3STE interacted strongly again with CESA 3 pPRESTE, as well with the N-terminally fused CESA 3 pPR3N. However, there was no strong interaction again between CESA1 and CESA3 if there was an N-terminal fusion.

This confirms previous results that at least in this yeast two hybrid, CESA1 and 3 do not strongly interact. Given the previous findings that CESA1 and 3 interact, it is possible that they require additional proteins for association, which is absent in a one to one membrane yeast two hybrid (Desperez *et al.,* 2007 and Wang and Elliot 2008). Desprez et al., 2007 suggested on the basis of their Bimolecular fluorescence complementation in tobacco leaves that interaction with native tobacco proteins cannot be ruled out. Wang and elliot, 2008 were able to successfully pull down an intact 840 kDA cellulose synthase complex, but even they suggested that there may be additional proteins in that complex yet to be detected. Further yeast 2 hybrid screens using the cloned baits with CESA1 and 3 described in this thesis will be required to find additional proteins. Additionally, further screens can be conducted using known genes required for cellulose synthesis. It would be interesting to test the cellulose interacting protein (CSI1) recently discovered by Gu *et al.* (2010) which is believed to be a scaffolding protein between CESAs. Also, we need to assess the interaction of CESA6 with the other CESAs, I hypothesize that CESA6 may mediate the interaction between CESA1 and 3.

6.0 Conclusions

A forward genetics approach was undertaken to isolate alleles coding for resistance to the cellulose biosynthesis herbicide flupoxam. It was initially hypothesized that flupoxam may target a similar albeit separate site observed in isoxaben resistant mutations (Vaughn and Turley, 2001). Indeed, genetic evidence for the mode of action of flupoxam suggests interaction with *CESA1* and *CESA3.* In literature, no mutation has been isolated on *CESA1* that does not show severe morphological phenotypes (Arioli *et al.,* 1998). Given the fact that alleles were isolated on separate genes, one can assume that flupoxam

disrupts a site shared by these two proteins. It was on this basis that a MbyTH was developed so as to possibly disrupt the interaction between CESA1 and CESA3 *in-vivo* using flupoxam. In doing so, it was shown that CESA1 and CESA3 interact exclusively with themselves and very weakly with each other. This is interesting given the abundance of literature suggesting otherwise (Desprez *et al*., 2007; Wang and Elliot, 2008). However, one cannot exclude the effect of endogenous proteins and membrane scaffolding that occur in-plant. Therefore, the MbyTH demonstrates a one-to-one recombinant approach to isolate new interacting proteins with the CESAs. Interestingly, a small screen using DET3, KORRIGAN and CTL1 demonstrated that CTL1 is a potentially weak interactor of CESA3. A larger scale approach could be employed using all potentially known cellulose deficient genes, and all possible combinations to piece together the entire cellulose synthase scaffold. More work needs to be done with respect to characterization of *fpx* mutants. For one, there are still remaining *fpx* mutants yet to be positionally cloned (**Table. 6**). Further characterization on the sugar profiles of *fpx* mutants needs to be pursued, as well as enzymatic hydrolysis to complement acid hydrolysis presented here. Much more work is needed with the MbyTH, including validation of all interactions through fractionation and western blotting. Finally, we need to test the interaction with CESA6 against CESA1 and 3.

7.0 References

Arioli, T., Peng, L., Betzner, A., Burn, J., Wittke, W., Herth, W., Camilleri, C., Hofte, H., Jaxek, P., Birch, R., Cork, A., Glover, J., Redmond, J., and Williamson, R. (1998). Molecular analysis of cellulose biosynthesis in *Arabidopsis.* Science. **279**, 717-720.

Barratt, D., Derbyshire, P., Findlay, K., Pike, M., Wellner, N., Lunn, J., Feil, R., Simpson, C., Maule, A., and Smith, A., (2009). Normal growth of *Arabidopsis* requires cytosolic invertase but not sucrose synthase. Proc. Natl. Acad. Sci. USA. **106,** 13124-13129.

Bartel, P., and Fields, S., (1995)**.** Analyzing protein-protein interactions using two-hybrid system. Methods Enzymol. **254,** 241-263.

Bressler, S., Gray, M., Sopher, B., Hu, Q., Hearn, M., Pham, D., Dinulos, M., Fukuchi, K., Sisodia, S., Miller, M., Disteche, C., and Martin, G, (1996). cDNA cloning and chromosome mapping of the human Fe65 gene: interaction of the conserved cytoplasmic domains of the human B-amyloid precursor protein and its homologues with the mouse Fe65 protein. Human Mol. Gen. **5,** 1589-1598.

Brett, C., (2000). Cellulose microfibrils in plants: biosynthesis, deposition, and integration into the cell wall. Int. Rev. Cytol. **199,** 161-199.

Brown, R., (1996). The biosynthesis of cellulose. J. Macromol. Sci. **33,** 406-421.

Burn, J., Hocart, C., Birch, R., Cork, A., and Williamson, R. (2002). Functional analysis of the cellulose synthase genes CesA1, CesA2, and CesA3 in Arabidopsis. Plant Physiol. **129**, 797-807.

Campagne, F., and Weinstein, H., (1999). Schematic representation of residue-based protein-context dependent data: an application to transmembrane data. Molecular Graphics and Modeling, **17,** 207-213.

Campange, F., and Weinstein, H., (2000). Iterative construction of residue-based diagrams of proteins: the RbDe web service. Protein Engineering, **13(6)**: 395-396.

Chen, S,. Ehrhardt, D., and Somerville, C., (2010). Mutations of cellulose synthase (CESA1) phosphorylation sites modulate anisotropic cell expansion and bidirectional mobility of cellulose synthase. Proc. Natl. Acad. Sci. **107,** 17188-17193.

Crowell, E., Bischoff, V., Desprez, T., Rolland, A., Stierhof, Y, Karin, S., Gonneau, M., Hofte, H., and Vernhettes, S. (2009). Pausing of golgi bodies on microtubles regulates secretion of cellulose synthase complexes in *Arabidopsis.* The Plant Cell. **21**, 1141-1154.

Daras, G., Rigas, S., Penning, B., Milioni, D., McCann, M., Carpita, N., Fasseas, C., and Hatzopoulos P., (2009). The *thanatos* mutation in *Arabidopsis thaliana* cellulose

synthase 3 (AtCesA3) has dominant-negative effect on cellulose synthesis and plant growth. New phytologist **184,** 114-126.

Desnos, T., Orboviv, V., Bellini, C., Kronenberger, J., Caboche, M., Traas, J., and Hofte, H. (1996). Procuste1 mutants identify two distinct genetic pathways controlling hypocotyl cell elongation, respectively in dark and light-grown Arabidopsis seedlings. Development. **122**, 683-693.

Desprez, T., Vernhettes, S., Fagard, M., Refregier, G., and Desnos, T. (2002). Resistance against herbicide isoxaben and cellulose deficiency caused by distinct mutations in the same cellulose synthase isoform CESA6. Plant physiol. **128**, 482-490.

Desprez, T., Juraniec, M., Crowell, E., Jouy, H., Pochylova, Z., Parcy, F., Hofte, H., Gonneau, M., and Vernhettes, S. (2007). Organization of cellulose synthase complexes involved in primary cell wall synthesis in *Arabidopsis thaliana.* Proc. Natl. Acad. Sci. **104(39),** 15572-15577.

Endler, A., and Persson, S., (2011). Cellulose synthases and Synthesis in Arabidopsis. Mol. Plant. **4,** 199-211.

Finley, L., and Brent, R., (1995). Interaction trap cloning with yeast. DNA cloning: a practical approach, Oxford University Press, pp 169-203.

Fujii, S., Hayashi, T., and Mizuno, K., (2010). Sucrose synthase as an integral component of the Cellulose synthase Machinery. Plant Cell Physiol. **51 (2),** 294-301.

Gietz, R., and Woods, R., (2002). Transformation of yeast by lithium acetate/single-stranded carrier DNA/polyethylene glycol method. Methods in enzymology, **350**, 87-96.

Gu, Y., Kaplinsky, N., Bringmann, M., Cobb, A., Carroll, A., Sampathkumar, A., Baskin, T., Persson, S., and Somerville, C., (2010). Identification of a cellulose synthase-associated protein required for cellulose biosynthesis. Proc. Natl. Acad. Sci. **107,** 12866-12871.

Harris, D., Seth, D., (2008)**.** Relative Crystallinity of Plant Biomass: Studies on Assembly, Adaptation and Acclimation. PLOS one. **8.**

Harris, D., Stork, J., and Debolt, S., (2009). Genetic modification in cellulose synthase reduces crystallinity and improves biochemical conversion to fermentable sugar. GCB Bioenergy. **1**, 51-61.

Hauser, M., Morikami, A., and Benfey, P., (1995). Conditional root expansion mutants of Arabidopsis. Development **121,** 1237-1252.

Heim, D., Skomp, J., Tschabold, E., and Larrinua, I. (1990). Isoxaben inhibits the synthesis of Acid insoluble cell wall materials in *Arabidopsis thaliana.* Plant Physiol. **93**, 0695-0700.

Hermans, C., Porco, S., Verbruggen, N., and Bush, D., (2010). Chitinase-like Protein CTL1 plays a role in altering root system architecture in response to multiple environmental conditions. Plant Phys. **152,** 904-917.

Herth, W., (1983) Arrays of plasma membrane "rosettes" in cellulose microfibril formation of spirogyra. Planta **159,** 347-358.

Hoffman, J., and Vaughn, K. (1996). Flupoxam induces classic club root morphology but is not a mitotic disrupter herbicide. Pesticide Biochem. and Physiol. **55**, 49-52.

Holland, N., Holland, D., Helentjaris, T., Dhugga, K., Xoconostle-Cazares, B., and Delmer D. (2000). A comparitive analysis of the plant cellulose synthase (CesA) gene family. Plant Physiol. **123**, 1313-1323.

Hu, S., Gao, Y., Tajima, K., Sunagewa, N., Zhou, Y., Kawano, S., Fujiwara, T., Yoda, T., Shimura, D., Satoh, Y., Munekata, M., Tanaka, I., and Yao, M., (2010). Structure of bacterial cellulose synthase subunit D octamer with four inner passageways. PNAS. **107**, 17957-17961.

Jarvis, M., (2000). Interconversion of the Iα and Iβ crystalline forms of cellulose by bending. Carb. Res. **325,** 150-154.

Kaida, R., Satoh, Y., Bulone, V., Yamada, Y., Kaku, T., Hayashi, T., and Kaneko, T., (2009). Activation of β-Glucan synthases by Wall-Bound Purple acid Phosphatase in Tobacco Cells. Plant Phys. **150,** 1822-1830.

Kimura, S., Laosinchai, W., Itoh, T., Cui, X., Linder, C., and Brown, R. 1999. Immunogold labeling of rosette terminal cellulose-synthesizing complexes in the vascular plant *Vigna angularis.* Plant Cell 11, 2075-85.

Konvicka, K., Campagne, F., and Weinstein, H., 2000. Interactive construction of residue-based diagrams of proteins: the RbDe web service. Protein engineering, **13(6)**, 395-396.

Li, X., Weng, J., and Chapple, C. (2008). Improvement of biomass through lignin modification. The plant journal. **54**, 569-581.

Miller, J. (1972)**.** Experiments in Molecular genetics. Cold Spring Harbour **p 352-355.**

Nagahashi, S., Sudoh, M, Ono, N., Sawada, R., Yamaguchi, E., Uchida, Y., Mio, T., Takagi, M., Arisawa, M., and Yamada-Okabe, H. (1995). Characterization of chitin synthase 2 of Saccharomyces cerevisiae. Impliciation of two highly conserved domains as possible catalytic sites. J. Biol. Chem. **270(23)**, 13961-13967.

Nakashima, K., Nishino, A., Horikawa, Y., Hirose, E., Sugiyama, J., Satoh, N., (2010). The crystalline phase of cellulose changes under developmental control in a marine chordate. Cell. Mol. Life Sci. Published online.

Nicol, F., His, I., Jauneau, A., Vernhettes, S., Canut, H., and Hofte, H., (1998). A plasma membrane-bound putative endo-1,4-β0gluanase is required for normal wall assembly and cell elongation in Arabidopsis. EMBO **17,** 5563-5576.

Nishiyama, Y., Langan, P., and Chanzy, H., (2002). Crystal structure and hydrogen-bonding system in cellulose Iβ from synchrotron X-ray and Neutron Fiber Diffraction. J.Am. Chem. Soc. **124,** 9074-9082.

Nishiyama, Y., Sugliyama, J., Chanzy, H., and Langan, P., (2003)**.** Crystal structure and hydrogen bonding system in Cellulose Iα from synchrotron X-Ray and Neutron Fiber Diffraction. J. Am. Chem. Soc. **125,** 14300-14306.

Nuhse, T., Stensballe, A., Jenson, O., and Peck, S. (2004). Phosphoproteomics of the *Arabidopsis* plasma membrane and a new phosphorylation site database. Plant Cell. **16**, 2394-2405.

Paradez, A., Somerville, C., and Ehrhardt, D. (2006). Visualization of cellulose synthase demonstrates functional association with microtubules. Science. **312**, 1491-1495.

Persson, S., Wei, H., Milne, J., Page, G., and Comerville, C. (2005). Identification of genes required for cellulose synthesis by regression analysis of public microarray data sets. Proc. Natl. Acad. Sci. **102**, 8633-8633.

Roudier, F., Fernandez, A., Fukita, M., Himmelspach, R., Borner, G., Schindelman, G., Song, S., Baskin, T., Dupree, P., Wasteneys, G., and Benfey, P. (2005). COBRA, an *Arabidopsis* extracellular glycosyl-phosphatidylinositol-anchored protein, specifically controls highly anisotropic expansion through its involvement in cellulose microfibril orientation. *Plant Cell.* **17**, 1749-1763.

Richmond, T., (2000). Higher plant cellulose synthases. Genome Biol. **4,** 30011-30016,

Sato, S., Kato, T., Kakegawa, K., Ishii, T., Liu, Y., Awano, T., Takabe, K., Nishiyama, Y., Kuga, S., Sato, S., Nakamura, Y., Tabata, S., and Shibata, D. (2001). Role of the putative membrane-bound endo-1,4-β-glucanase KORRIGAN in cell elongation and cellulose synthesis in *Arabidopsis thaliana.* Plant Cell Physiol. **42**, 251-263.

Saba, R., and Vaughn, K., (1999). Herbicides that inhibit cellulose biosynthesis. Weed Science **47,** 757-763.

Sambrook, J., and Russel, D., (2001)**.** Molecular Cloning A laboratory Manual. 3rd edition. Cold Spring Harbor press, New York.

Samuels, M., and Witmer, J., (2003). Statistics for life sciences 3rd edition. Pearson Education Inc.

Saxena, I., Brown, R., and Dandekar, T. (2001). Structure-function characterization of cellulose synthase: relationship to other glycosyltransferases. Phytochem. **57**, 1135-1148.

Segal, L., Creely, J., Martin, A., and Conrad, C., (1959). An empirical method for Estimating the Degree of Crystallinity of Native Cellulose using the X-Ray Diffractometer. Textile Research Journal, **29,** 786-794.

Sheible, W., Eshed, R., Richmond, T., Delmer, D., and Somerville, C. (2001). Modifications of cellulose synthase confer resistance to isoxaben and thiazolidinone herbicides in Arabidopsis Ixr1 mutants. Proc. Natl. Acad. Sci. **98,** 10079-10084.

Somerville, C. (2006). Cellulose synthesis in Higher Plants. Annu. Rev. Cell Dev. Biol. **22**, 53-78.

Stagljar, I., Korostensky, C., Johnsson, N., and TeHeesen, S., (1998). A genetic system based on split-ubiquitin for the analysis of interactions between membrane proteins in vivo. *Proc. Natl. Acad. Sci.* **95,** 5187-5192.

Sticklen, M., (2006). Plant genetic engineering to improve biomass characteristics for biofuels. Current Opinion Biotech. **17,** 315-319.

Taylor, N., (2007). Identification of cellulose synthase AtCesA7 (IRX3) in vivo phosphorylation sites—a potential role in regulating protein degradation. Plant Mol. Biol. **64,** 161-171.

Timmers, J., Vernhettes, S., Depsrez, T., Vincken, J., Visser, R., and Trindade, L., (2009). Interactions between membrane-bounds cellulose synthases involved in the synthesis of the secondary cell wall. FEBS **583,** 978-982.

Thaminy, S., Miller, K., and Stagljar, I., (2006). The Split-Ubiquitin Membrane-Based Yeast two-Hybrid System. Methods in Mol. Biol. **261,** pg 297-312.

Turner S., and Somerville, C., (1997). Collapsed xylem phenotype of Arabidopsis identifies mutants deficient in cellulose deposition in the secondary cell wall. Plant Mol. Biol. **47,** 209-219.

Updegraff, D. (1969). Semimicro determination of cellulose in biological materials. Anal. Biochem. **32(3)**, 420-424.

Vaughn, K., and Turley, R., (2001). Ultra structural effects of cellulose biosynthesis inhibitor herbicides on developing cotton fibers. Protoplasma **216,** 80-93.

Wang, J., Elliot, J., and Williamson, R., (2008). Features of the primary wall CESA complex in wild type and cellulose-deficient mutants of Arabidopsis thaliana. Journal of Exp. Bot. **59,** 2627-2637.

Xu, F., and Joshi, C., (2010). *Invitro* demonstration of interactions among zinc-binding comains of cellulose synthases in *Arabidopsis* and aspen. Advanc. Bios. and Biotech. **1,** 152-161.

8.0 List of Figures

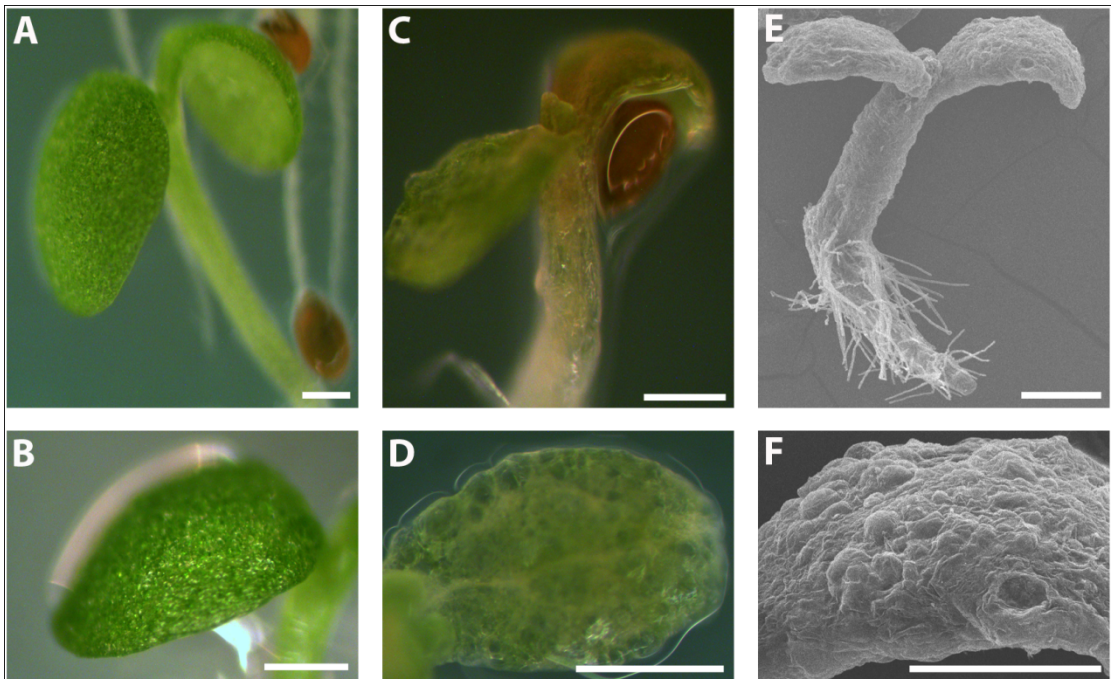

Figure 1. Effect of 5 nM flupoxam on *Arabidopsis thaliana* landberg ecotype. Light microscope picture of Landsberg *Arabidopsis thaliana* hypocotyl and cotyledon grown on MS (**A, B)** is compared to the same ecotype grown in the presence of 5 nM flupoxam (**C, D, E, F).** Blebbing cell structure is visualized better using a Scanning electron micrograph (**E, F).** White bar represents 1 mm.

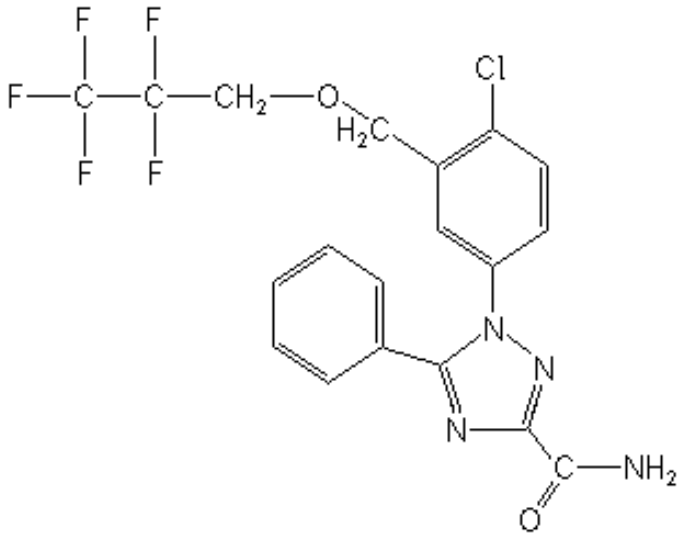

Figure 2. Chemical Structure of flupoxam [1-[4-chloro-3-(2,2,3,3,3-pentafluoropropoxymethyl)phenyl]-5-phenyl-1*H*-1,2,4-triazole-3-carboxamide].

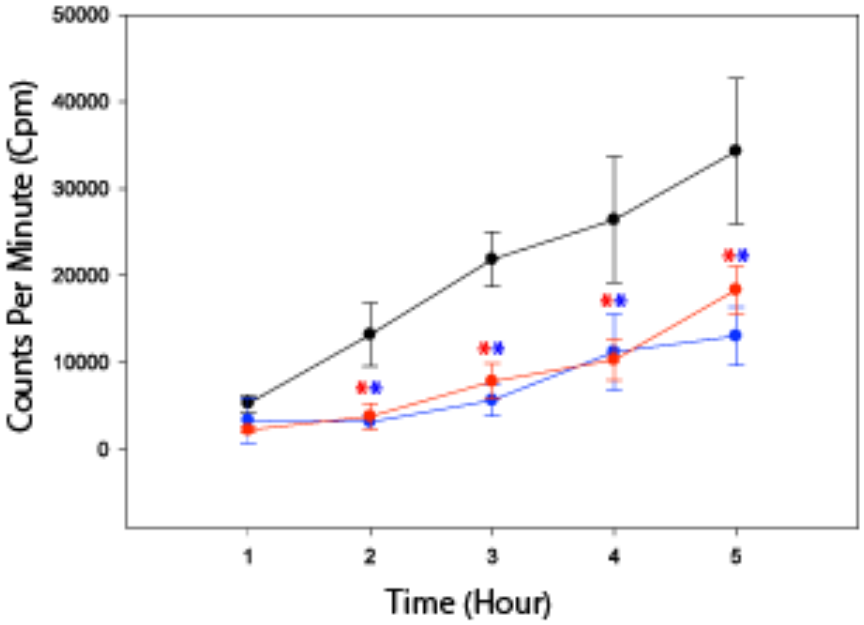

Figure 3. C^{14} incorporation into 5 day old seedlings- Insoluble cellulosic measurements of seedlings expressed as counts per minute (cpm). Measurements are the result of 1hour C^{14}-glucose incorporation seedlings after 5 days of dark growth on MS and then incubated in either in the presence/absence of herbicide. ● - Ethanol control + C^{14}-glucose, ● - 1 µM Flupoxam + C^{14}-glucose . ● - 1 µM Isoxaben + C^{14}-glucose. Errors bars represent +/- SD. * represents significance in comparison to the control non-treated according to

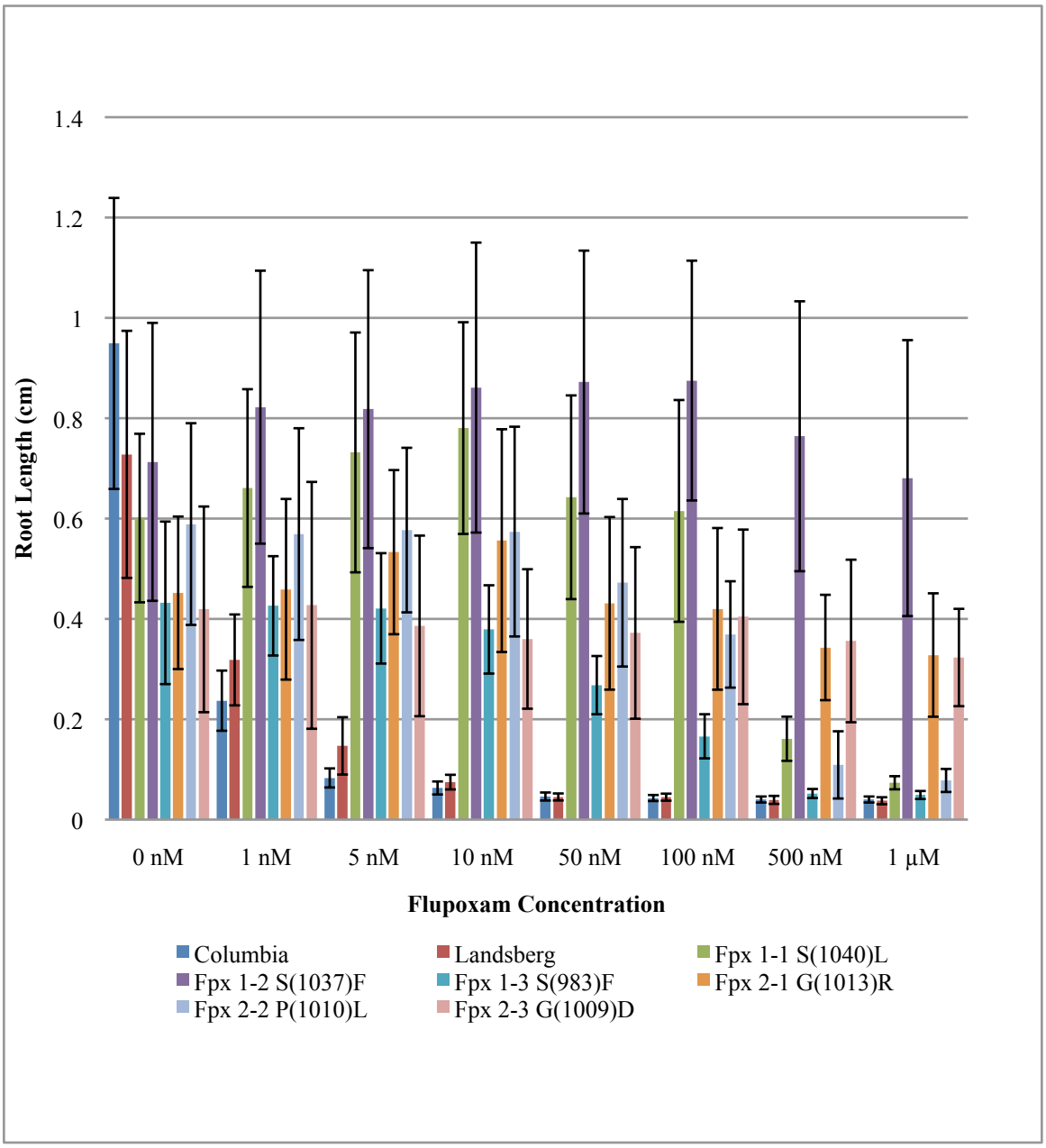

Figure 4. Chemical resistance to the herbicide flupoxam for cellulose synthase 1 and 3 mutations. Root length measurements (cm) were assessed with increasing concentrations of flupoxam are shown (n=100) following 5 days of growth and measured using Macnification.

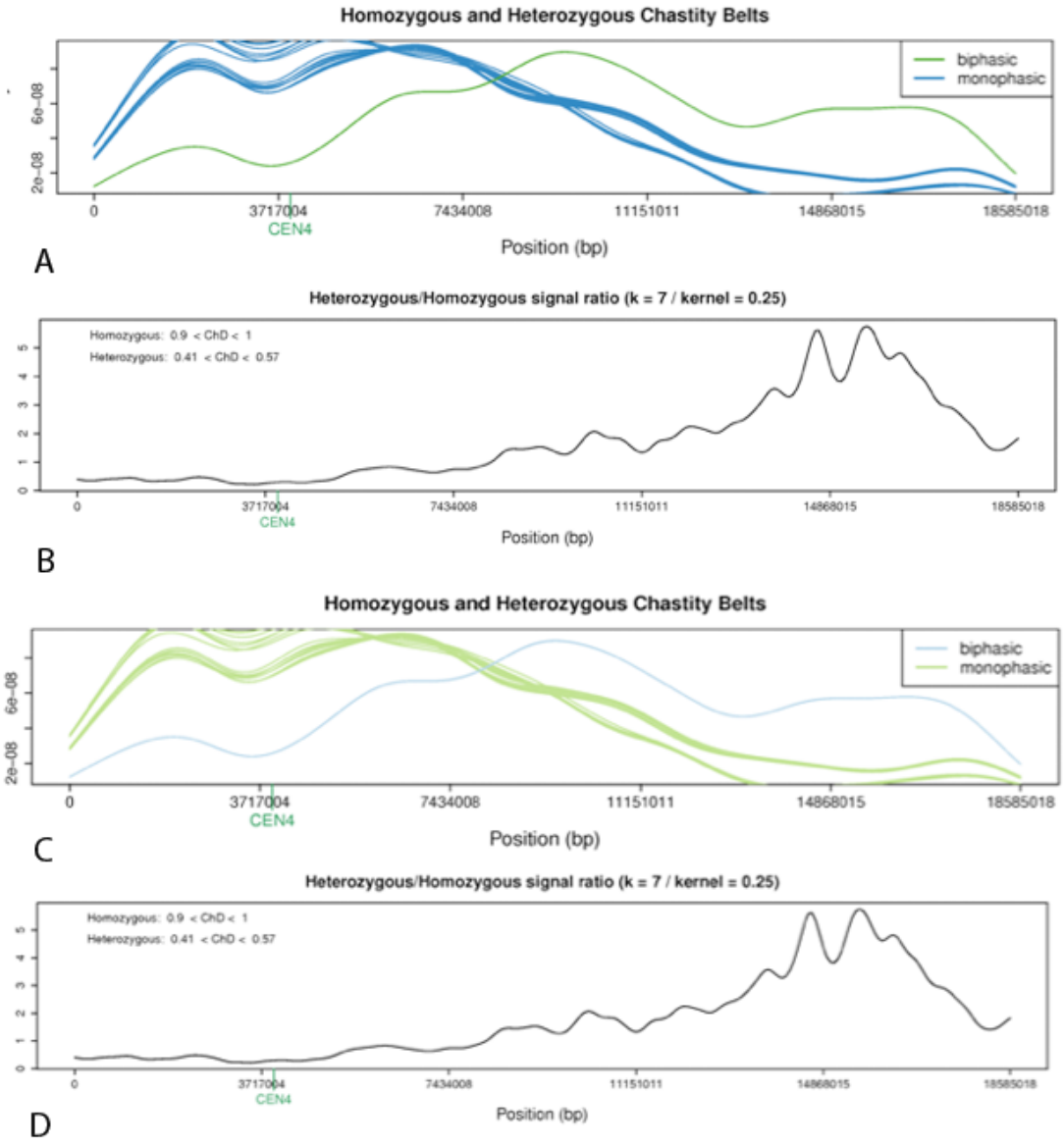

Figure 5. Next-generation mapping chastity belts for *fpx* 2-2, *fpx* 2-3 along chromosome 4. The chastity belts for *CESA1*$^{Fpx\ 2\text{-}3}$ **(A,B)** and *CESA1*$^{Fpx\ 2\text{-}2}$ **(C,D)** are shown. **(A,C)** represent the ratio of homozygousity (biphasic) compared to the heterozygousity (monophasic). **(B,D)** represent the refinement in the chastity statistic by decreasing kernal size, ie. The region of highest divergence in chastity statistic along chromosome 4.

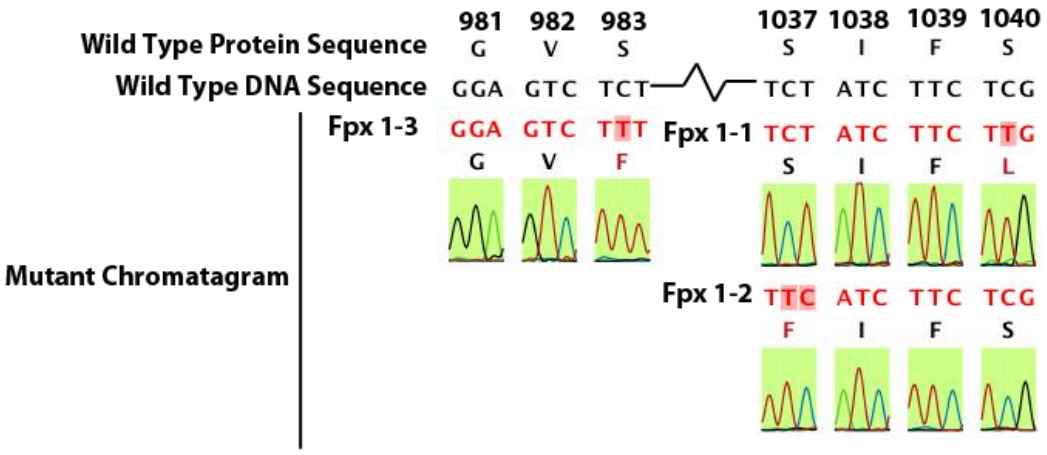

Figure 6. DNA chromatograms for cellulose synthase 3 mutations. Numbers at the top represent relative amino acid substitutions on *CESA* 3 (At5G05170). EMS generated polymorphism is indicated by the red highlighted base pair change as compared to wild-type Columbia sequence. In the case of *fpx* 1-2, the third base of the codon change represents a landsberg silent polymorphism, while the second base change is the EMS generated mutation.

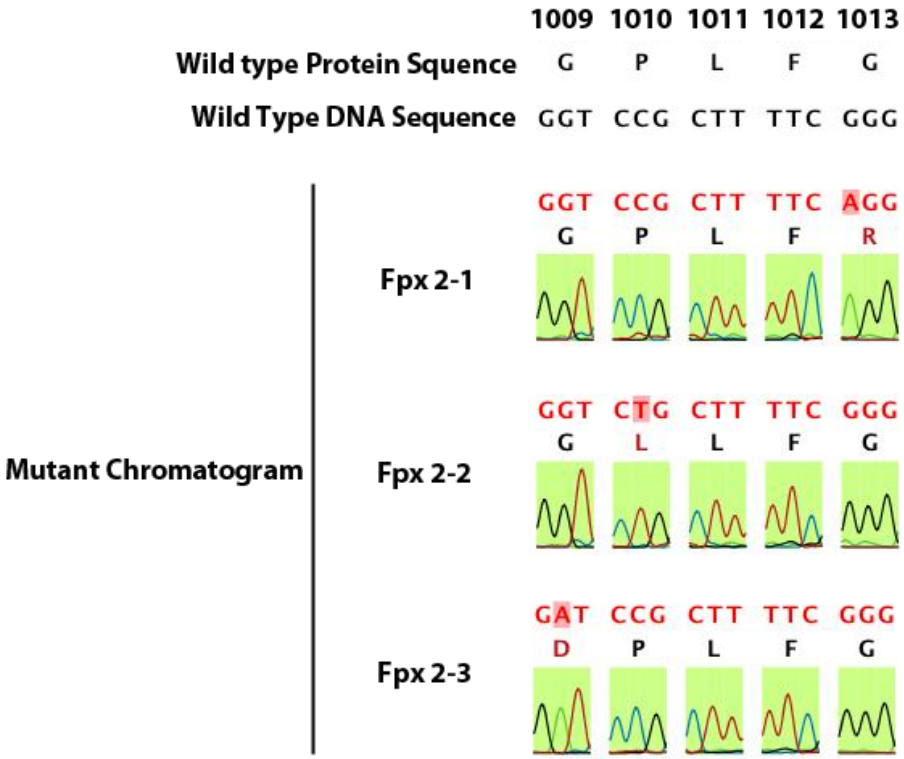

Figure 7. DNA chromatogram for cellulose synthase 1 mutations. Numbers at top represent respective amino acid subtitutions on *CESA*1 (At4G32410). EMS generated DNA polymorphisms pertaining to flupoxam resistance are indicated as the red highlight base pair change as compared to Columbia wild type sequence.

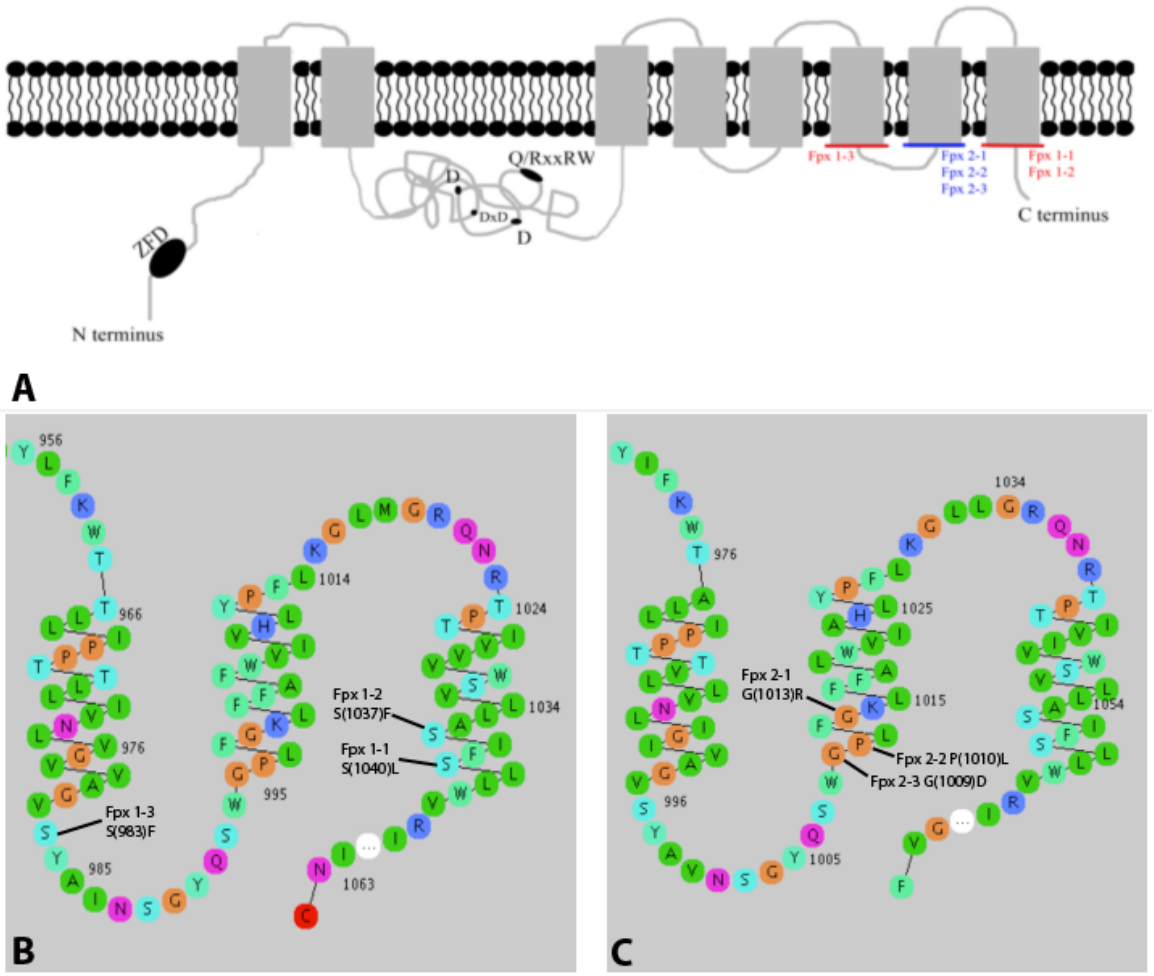

Figure 8. Relative CesA Protein position using Residue based diagram editor.

General superimposition of cellulose synthase mutations is shown in (**A).** A residue based diagram editor (RbDe) shows the relative predicted location of transmembrane amino acids in CesA 3 (**B)** and CesA 1 (**C).**

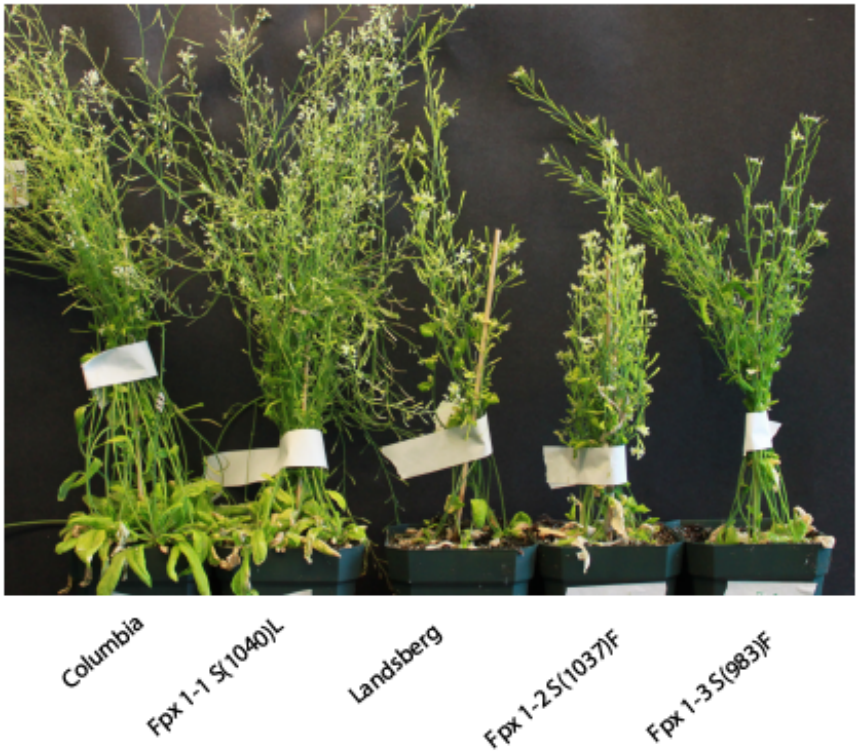

Figure 9. Adult CESA3 Mutants. Mutations as indicated are compared to their respective backgrounds Columbia for CESA3$^{Fpx\ 1\text{-}1}$ and Landsberg for CESA1$^{Fpx\ 1\text{-}2,\ Fpx\ 1\text{-}3}$ (n=~6).

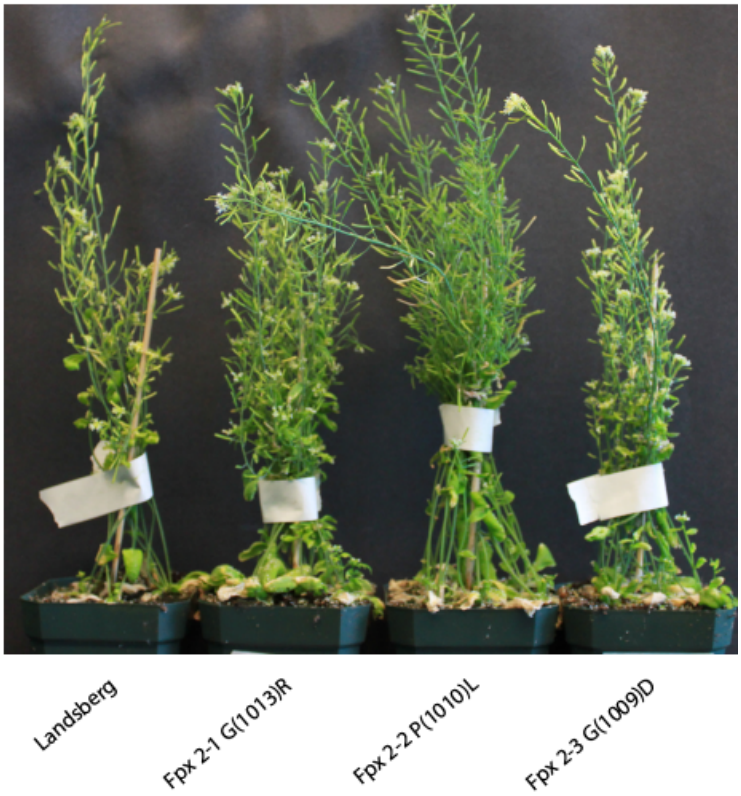

Figure 10. Adult CESA 1 Mutants. Mutations as indicated are compared to wild type Landsberg (n=~6).

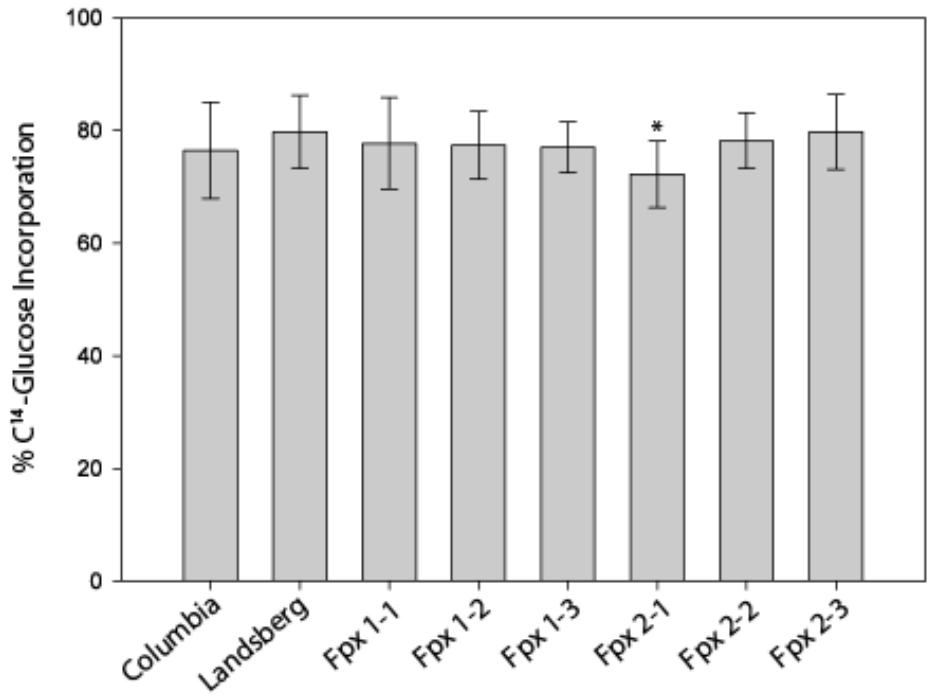

Figure 11. Percent C^{14} -glucose incorporation in mutants. Incorporation of C^{14}-Glucose was examined to look at the effect mutations on glucose incorporation into the cellulosic fraction. (n=~20) Mutants were compared to wild type controls and were determined significant according to a Dunnett One-Way Anova ($p<0.05$).

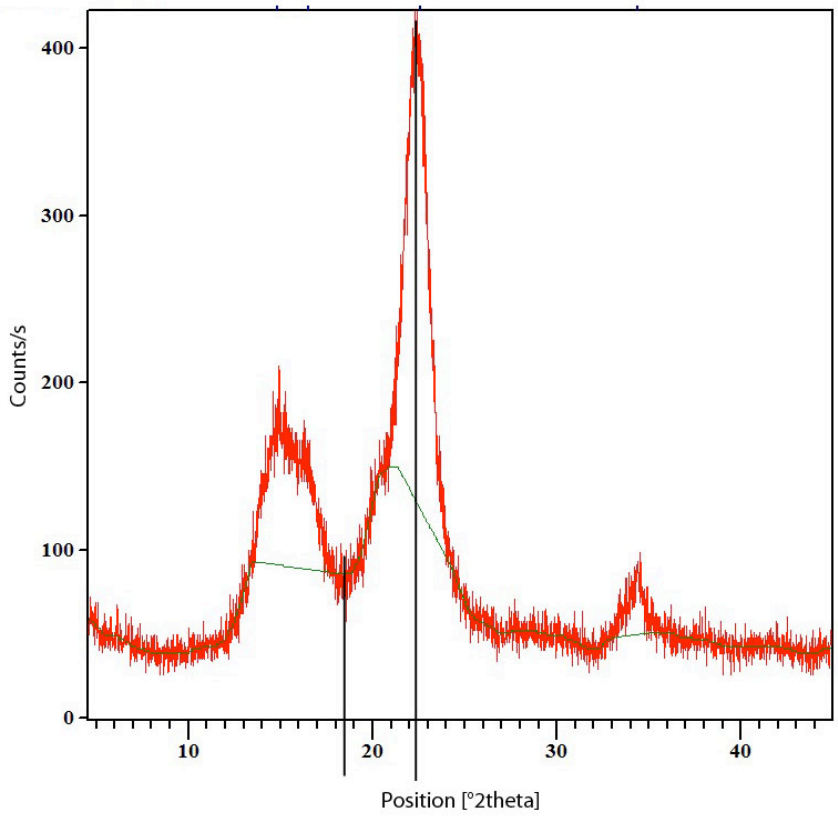

Figure 12. X-Ray diffraction diagram of pure cellulose. X-ray diffraction of pure cellulose (Sigma-Alrich; St.Louis, MO) show crystalline peak around 22.5° and amorphous trough around 18° 2θ as previously shown (Segal *et al.*, 1959).

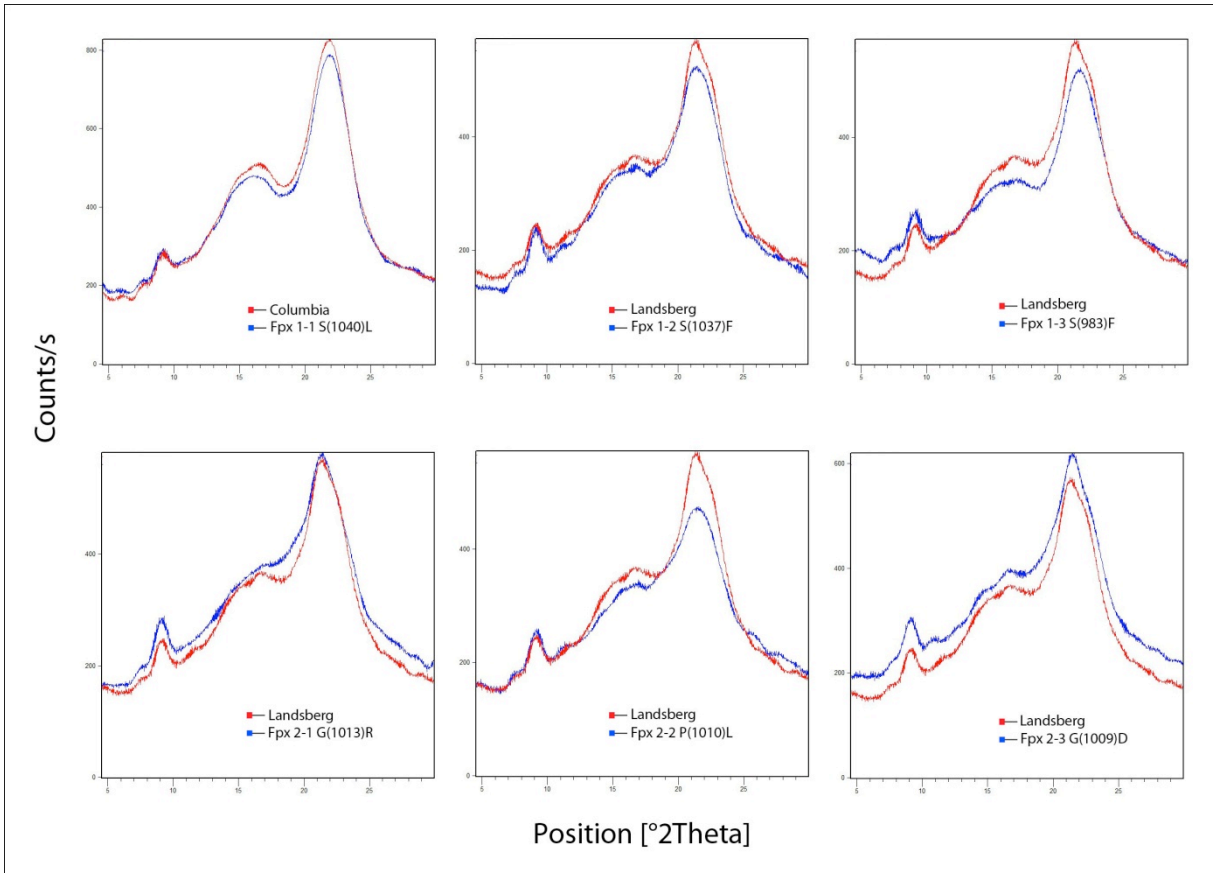

Figure 13. X-Ray Diffraction diagrams for cellulose synthase mutations. X-ray diffraction diagrams of wild type *Arabidopsis thaliana* tissue are compared to diffraction diagrams for amino acid substitutions.

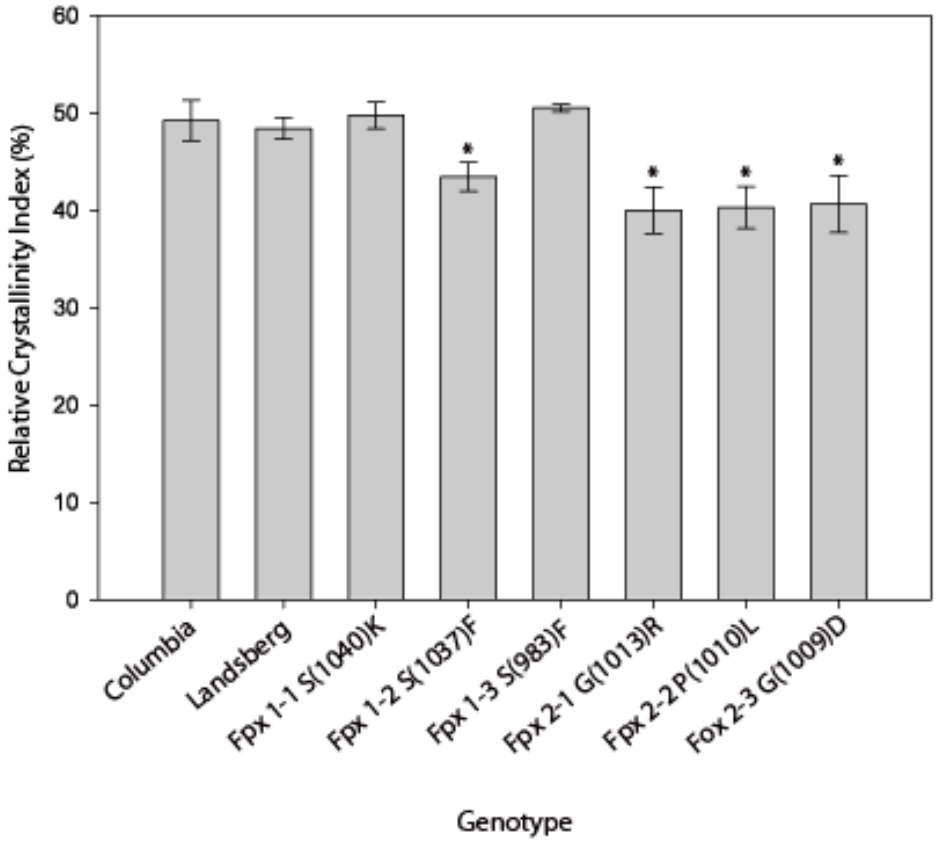

Figure 14. Relative crystallinity index (RCI) of Dry tissue. The relative crystallinity index (RCI) of wild type as well as mutants are compared (n=3). * determined significant via a Dunnett One-Way Anova.

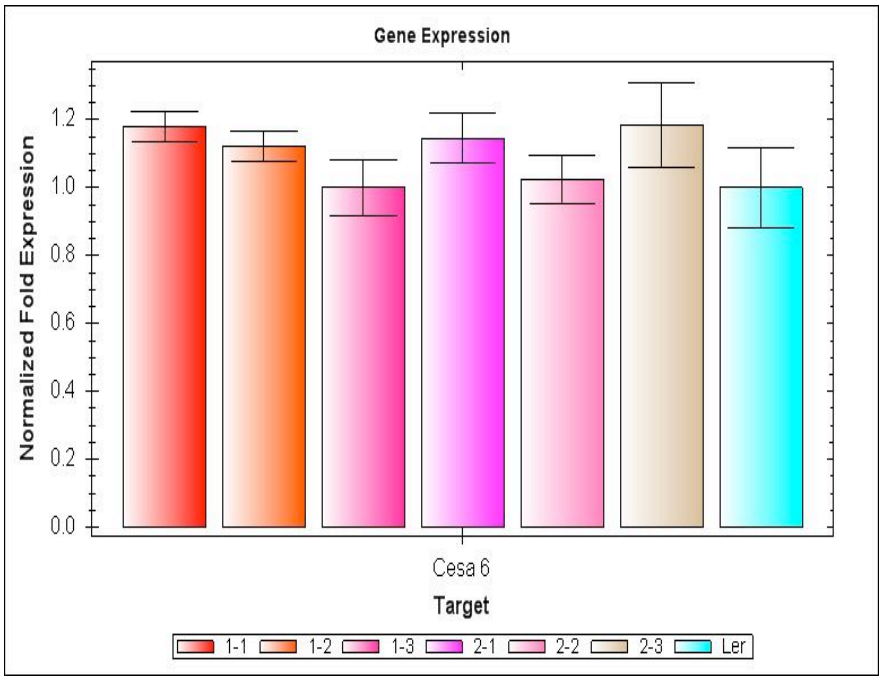

Figure 15. *CESA* 6 expression. *CESA* 6 expression (n=3 biological replicates) for all the mutants compared to Landsberg was measured using qRT-PCR.

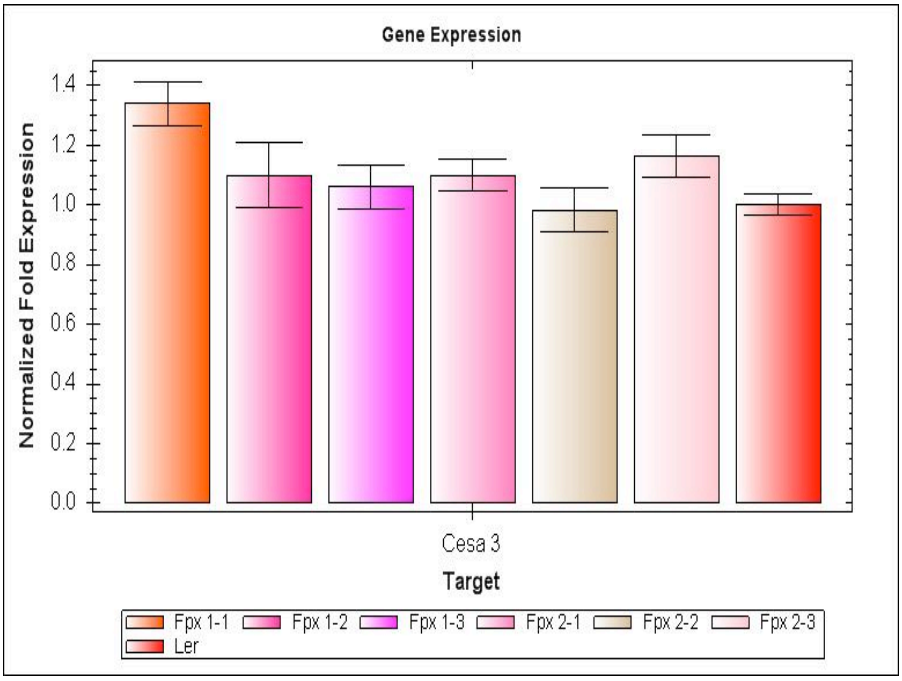

Figure 16. *CESA*3 Expression. *CESA*3 expression (n=3 biological replicates) for all the mutants compared to Landsberg was measured using qRT-PCR.

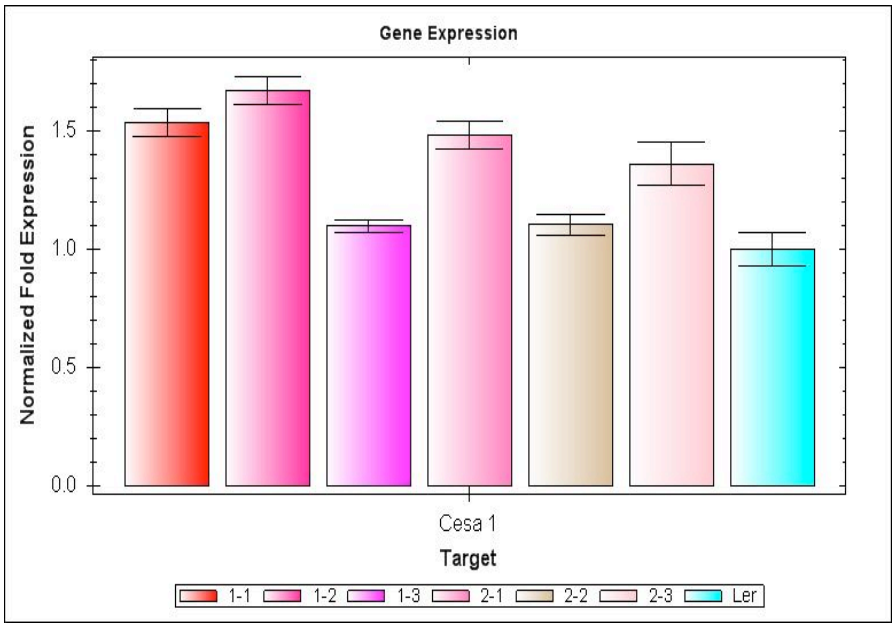

Figure 17. *CESA*1 Expression. *CESA*1 expression (n=3 biological replicates) for all the mutants compared to Landsberg was measured using qRT-PCR.

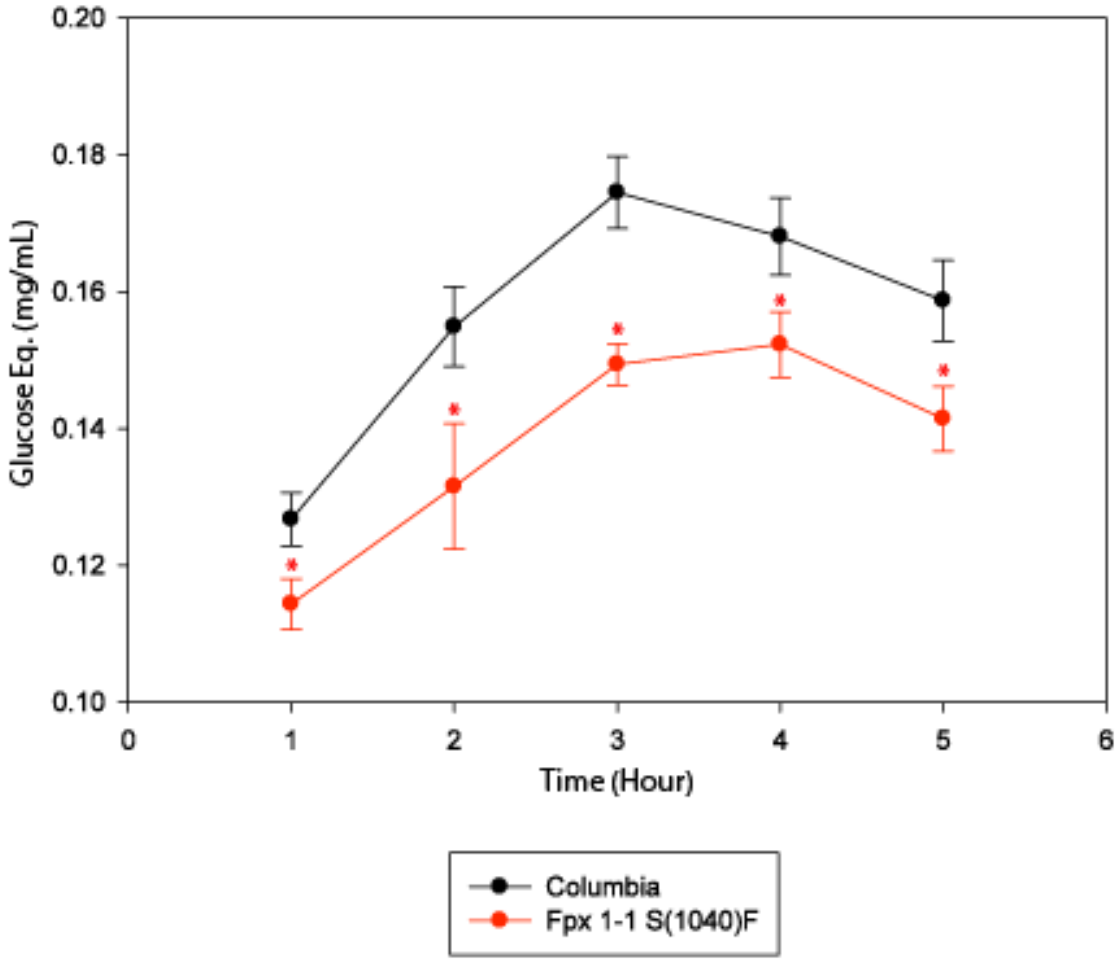

Figure 18. Anthrone Sugar Determination Fpx 1-1

A time course acid hydrolysis and anthrone sugar determination on CESA 3$^{\text{Fpx 1-1}}$ S(1040)L is compared to a Columbia control (n=6). * Determined significant in comparison to control ($p<0.05$) according to a dunnett one way anova.

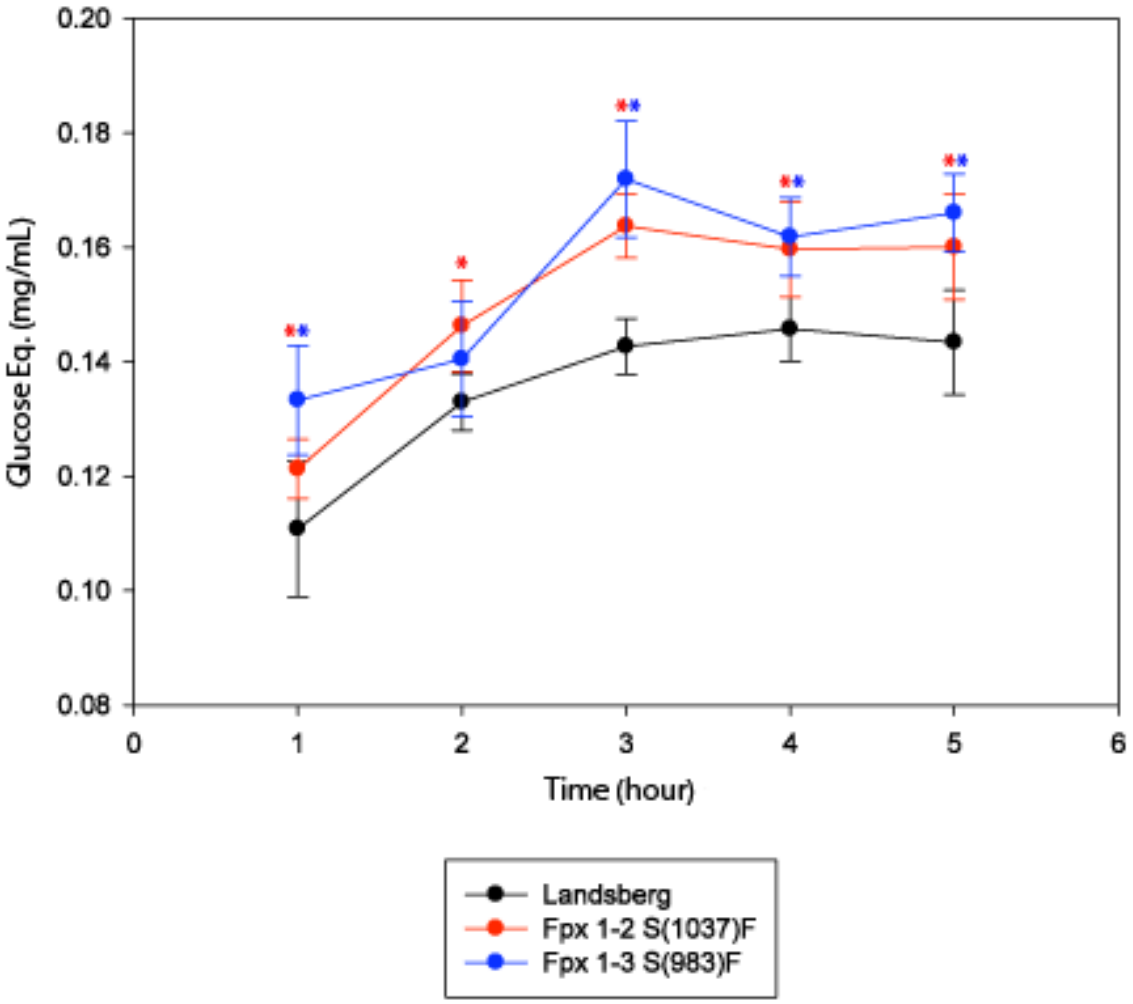

Figure 19. Anthrone Sugar determination *fpx* 1-2 and *fpx* 1-3.

A timecourse acid hydrolysis-anthrone sugar determination on CESA3$^{Fpx\ 1\text{-}2}$ S(1037)F and CESA3$^{Fpx\ 1\text{-}3}$ S(983)F is compared to a Landsberg control (n=6). * Determined significant in comparison to control ($p<0.05$) according to a dunnett one way anova.

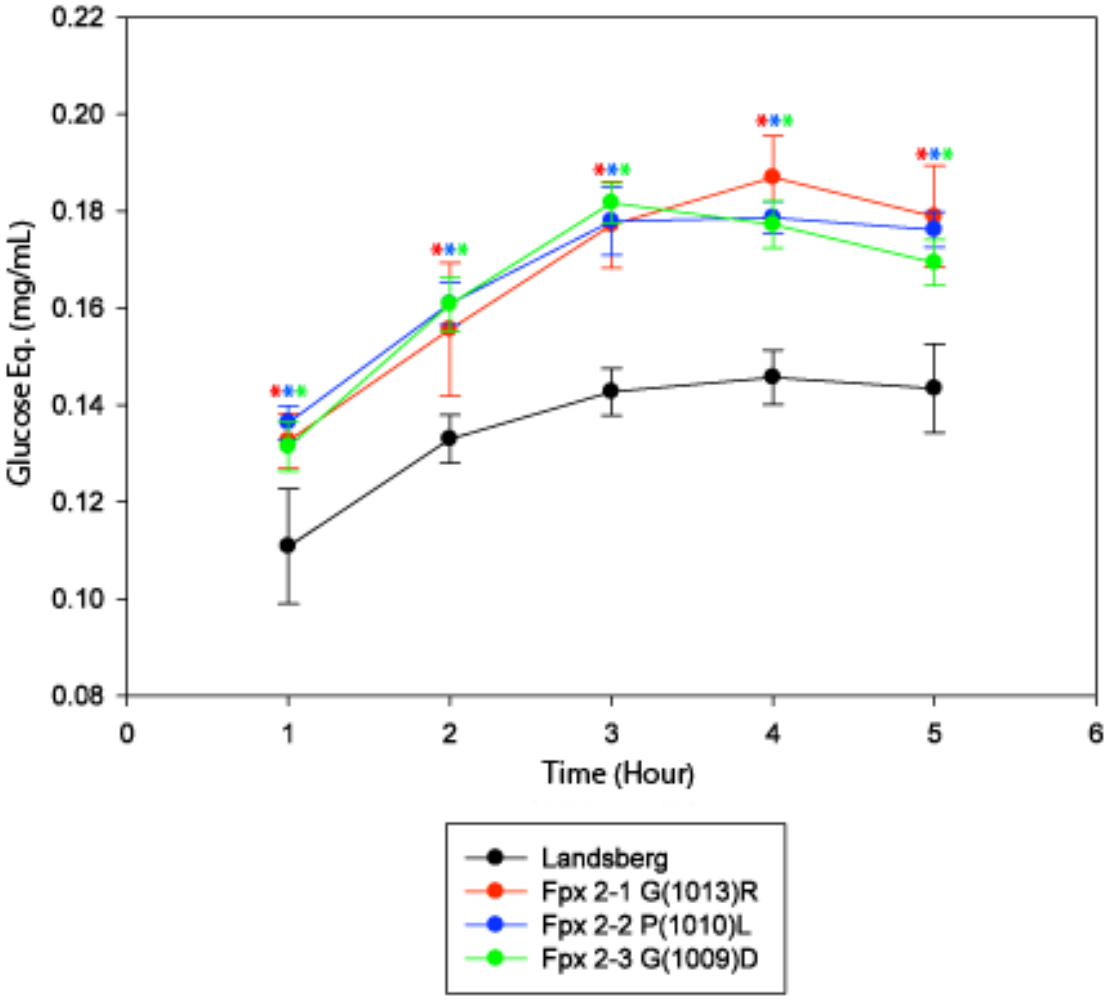

Figure 20. Anthrone sugar determination *fpx* 2-1, *fpx* 2-2 and *fpx* 2-3.

A time course acid hydrolysis and anthrone sugar determination on CESA $1^{Fpx\ 2\text{-}1}$ G(1013)R, CESA $1^{Fpx\ 2\text{-}2}$ P(1010)L, and CESA $1^{Fpx\ 2\text{-}3}$ G(1009)D is compared to a Landsberg control (n=6). * Determined significant in comparison to control ($p<0.05$) according to a dunnett one way anova.

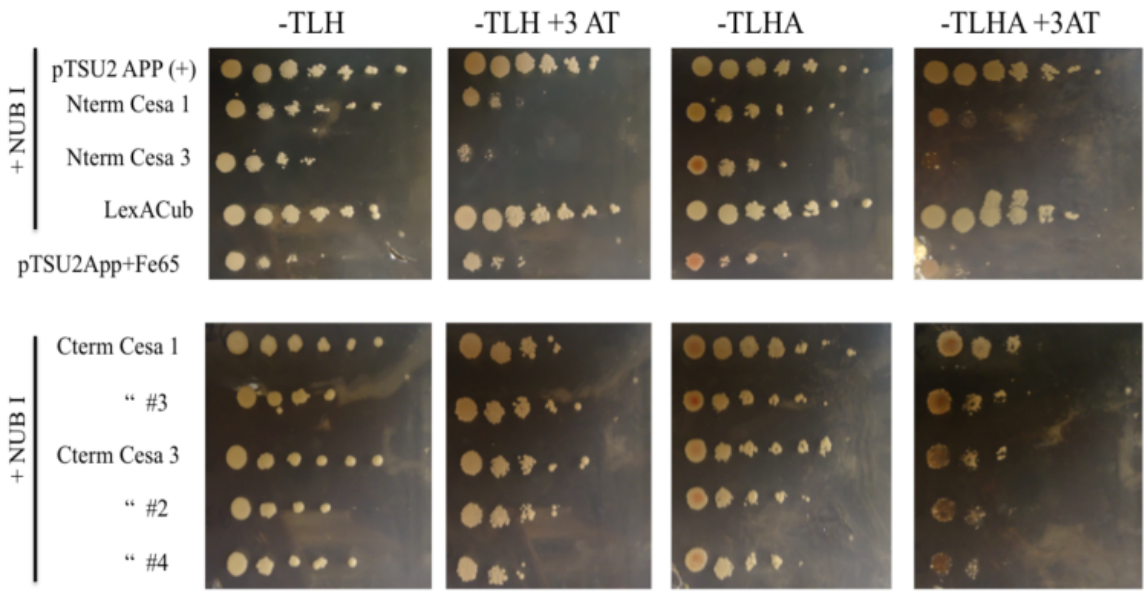

Figure 21. C-terminal vs N-terminal fusions in MbyTH.

N-terminal fusions of with CESA1 and 3 using plasmid pBT3-N are compared to C-terminal fusions using plasmid pBT3STE with the same genes. Numbers represent clone replicates.

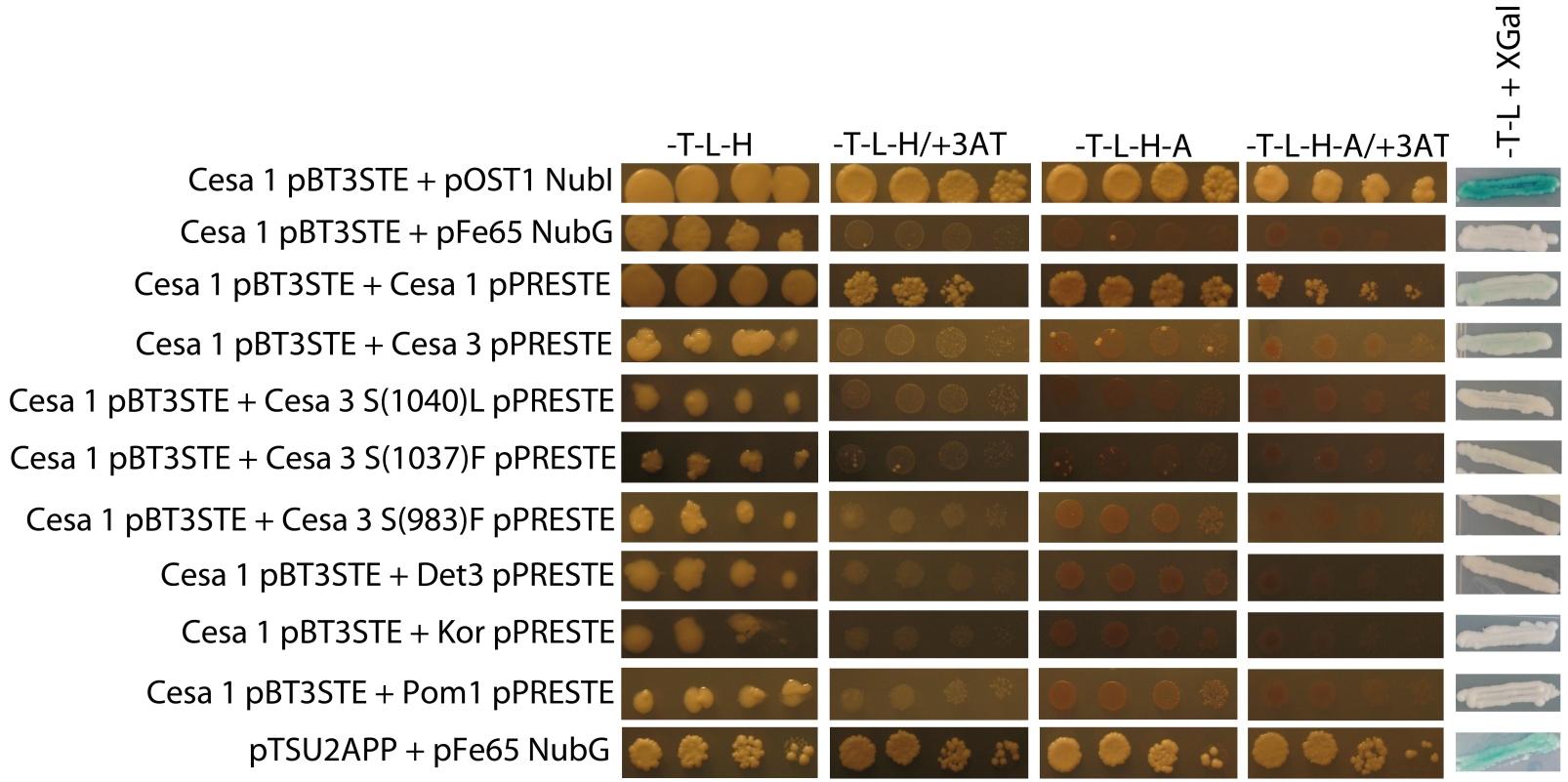

Figure 22. Membrane Yeast 2 Hybrid using CesA 1 pBT3STE. Co-transformations are indicated on the left. Relative strength of interaction was assessed on standard dropout media lacking –T(Tryptophan)-L(Leucine) to maintain plasmids, and –H(Histidine) and –A(Adenine) to test the relative strength of interaction. +3 AT represents the addition of 10 mM 3-Amino-Triazole. Expression of β-Galactosidase is assessed by addition of X-Gal(blue=strong).

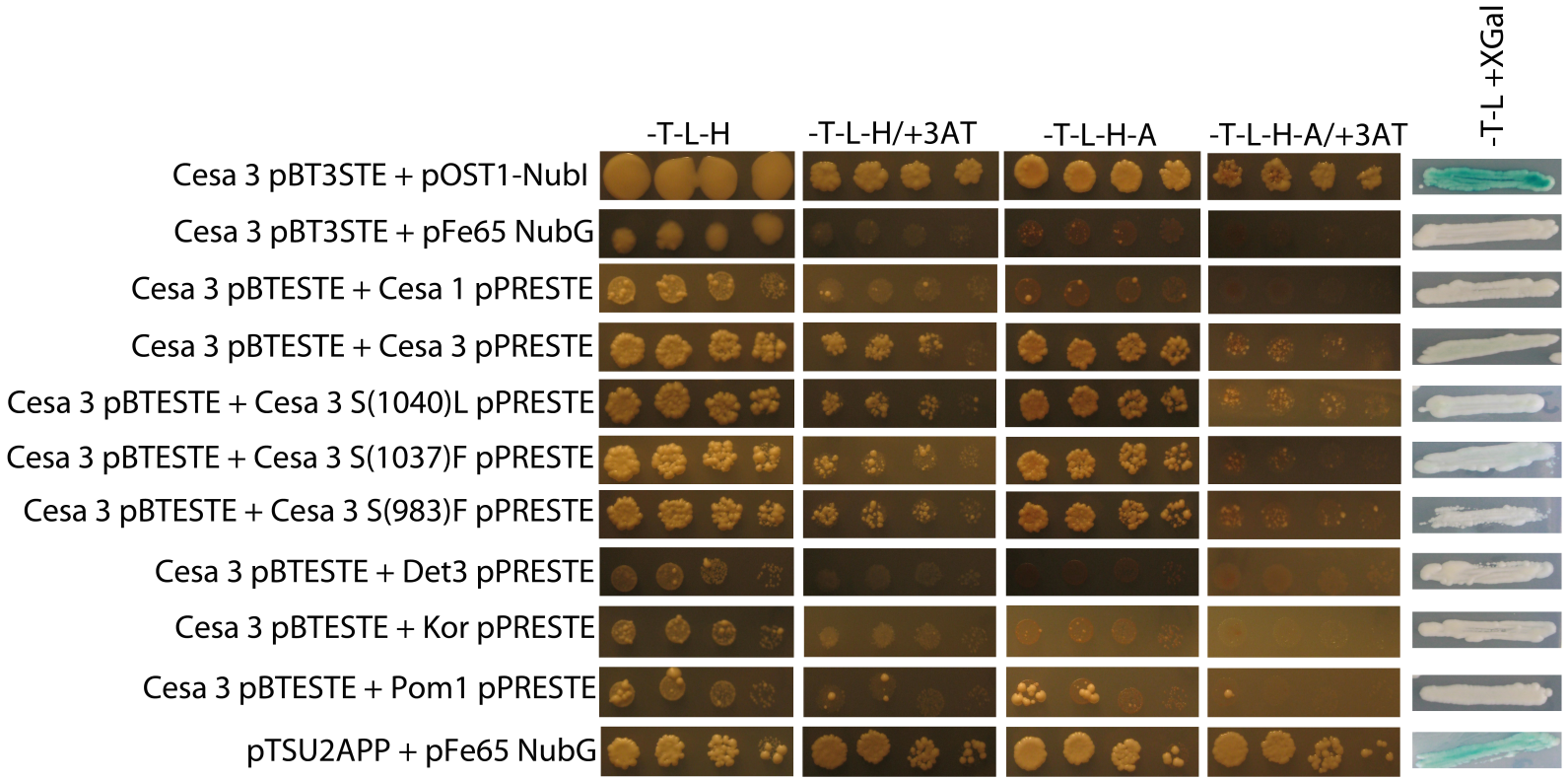

Figure 23. Membrane Yeast 2 Hybrid using CesA 3 pBT3STE. Co-transformations are indicated on the left. Strength of interaction was assessed as previously described.

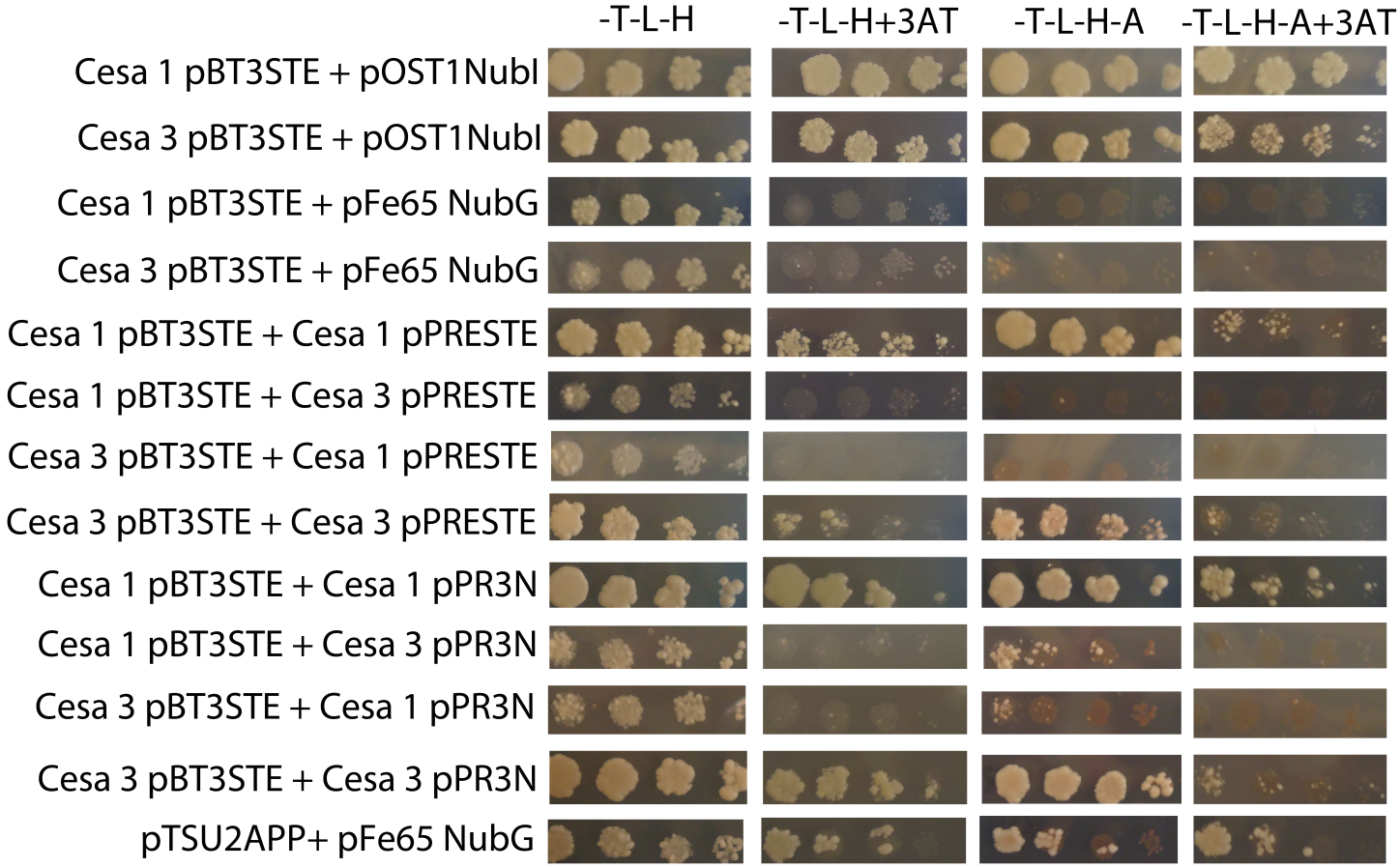

Figure 24. CESA 1/3 pBT3STE tested against N-terminal Preys (pPR3N). Co-transformation are indicated on the left with relative strength of interaction assessed by method previously described.

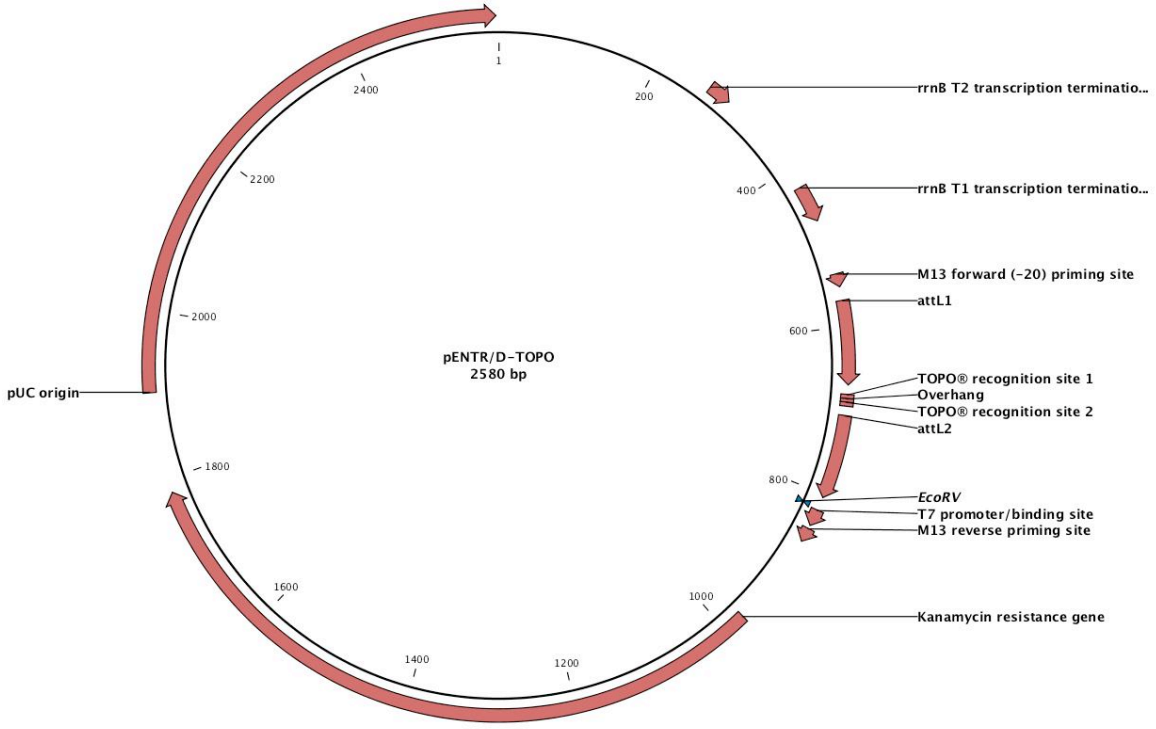

Figure 25. pENTR/D-TOPO Plasmid Map.

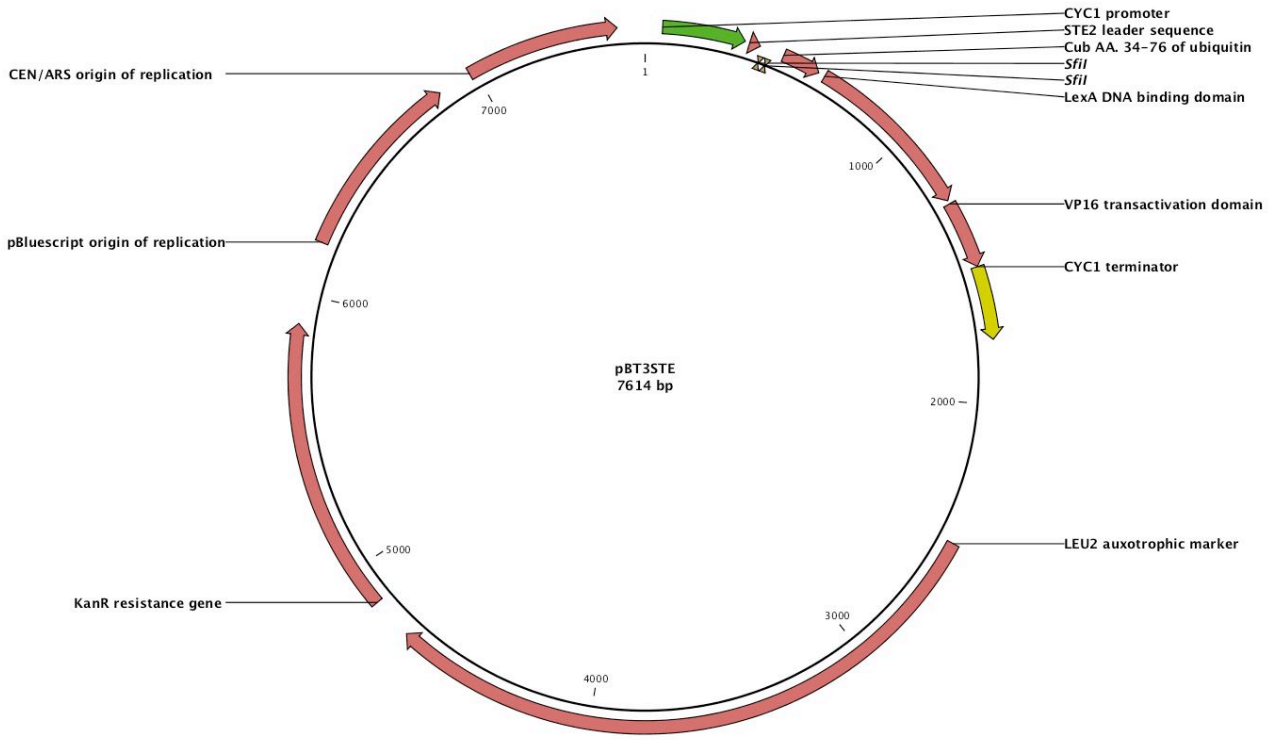

Figure 26. pBT3STE Plasmid Map.

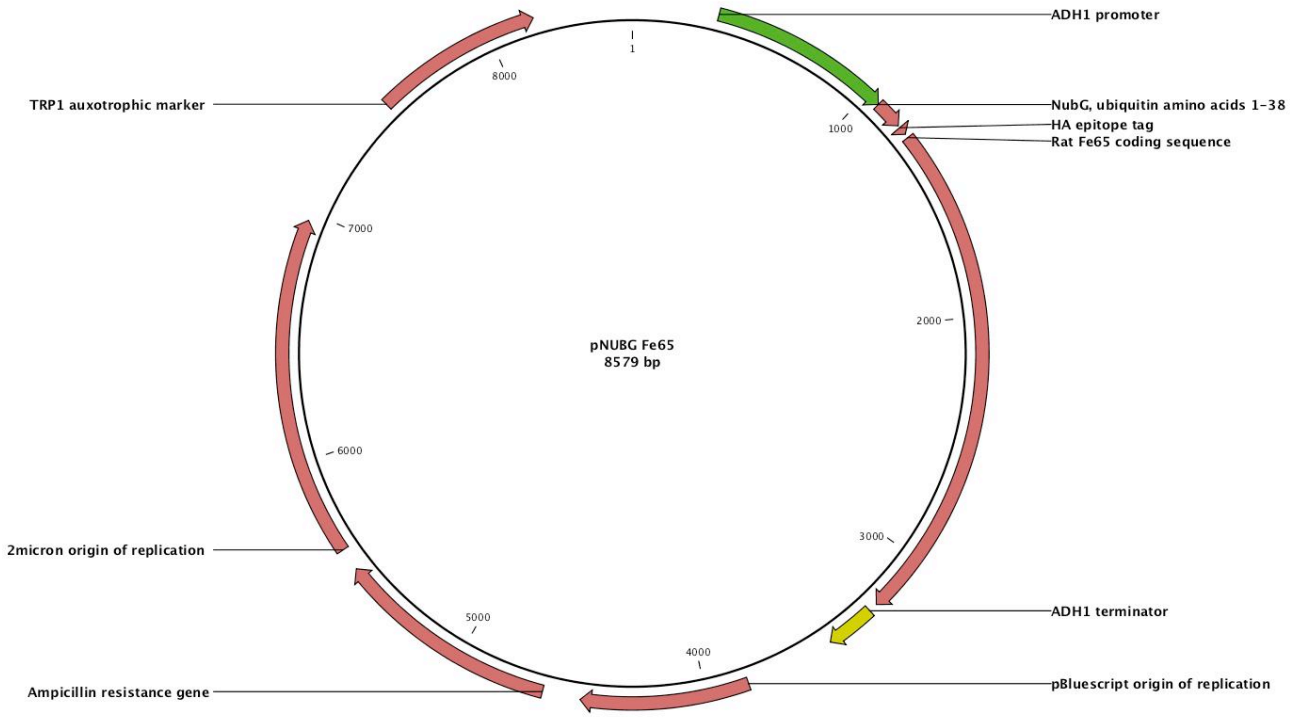

Figure 27. pFe65 NubG Plasmid Map.

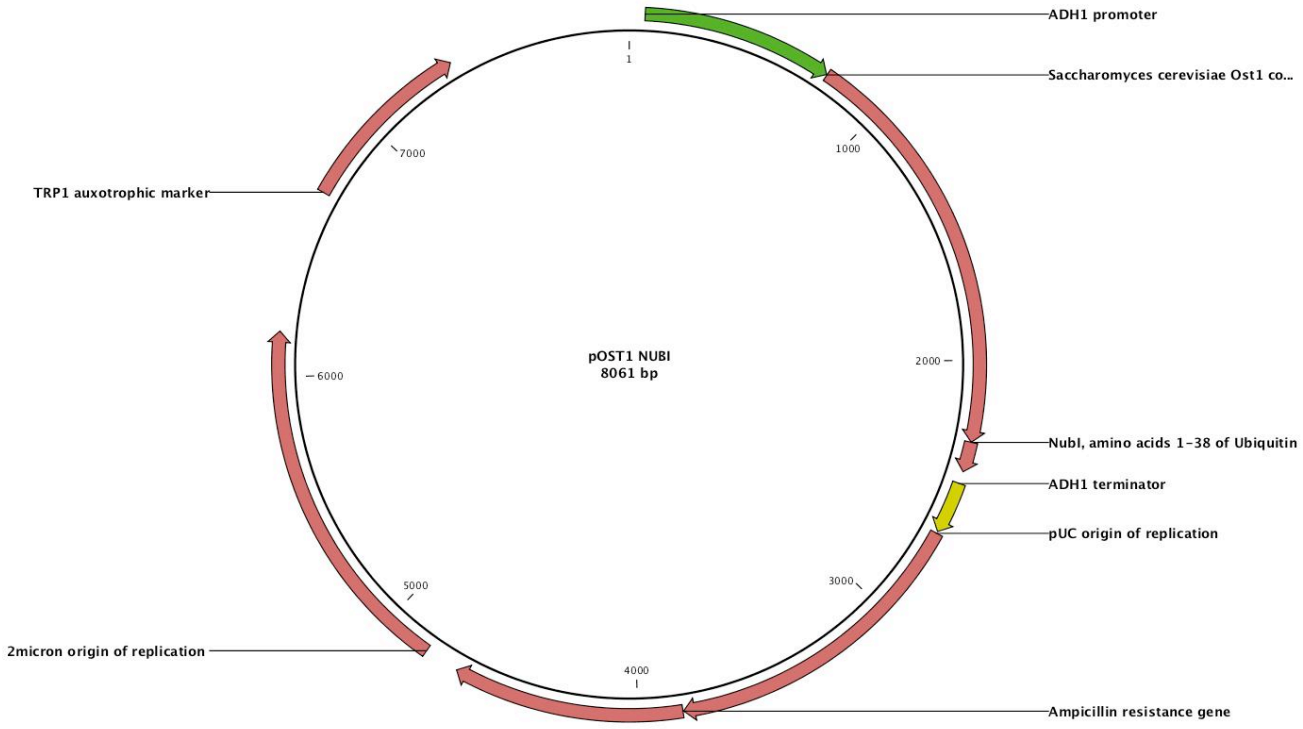

Figure 28. pOST1 NubI Plasmid Map.

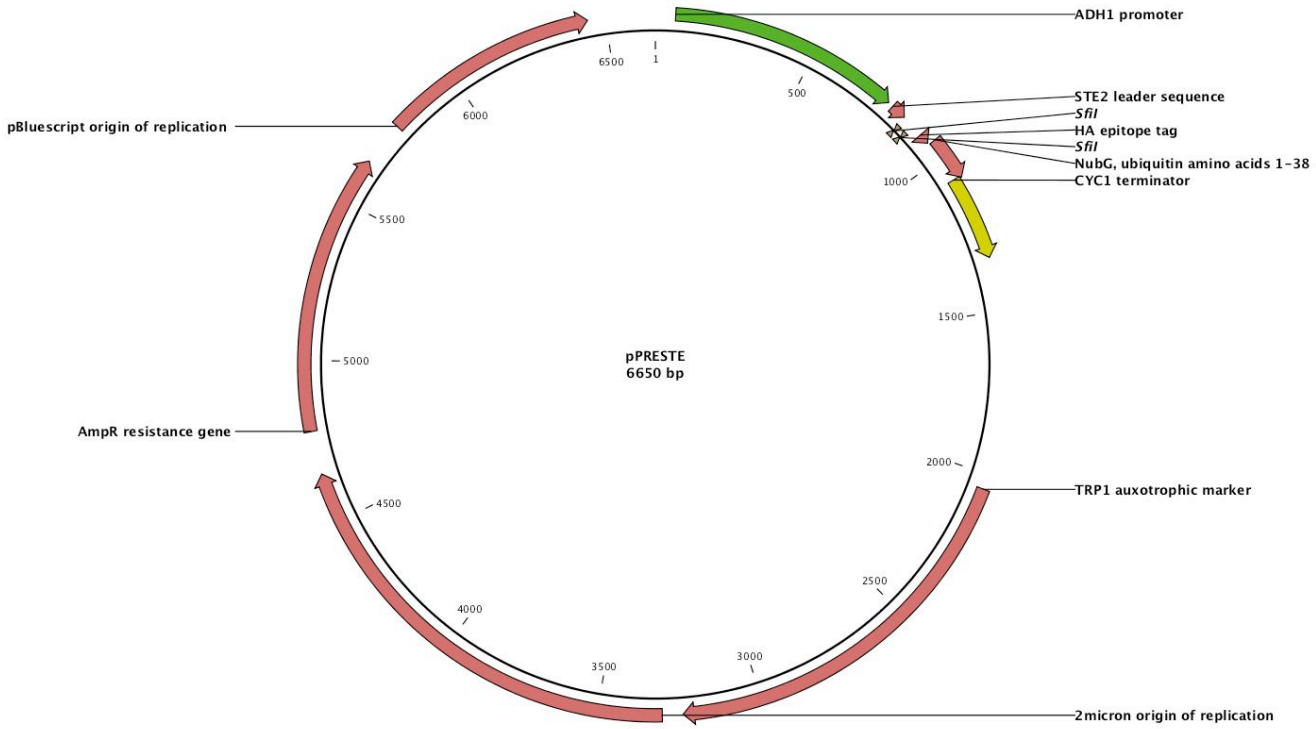

Figure 29. pPRESTE Plasmid Map.

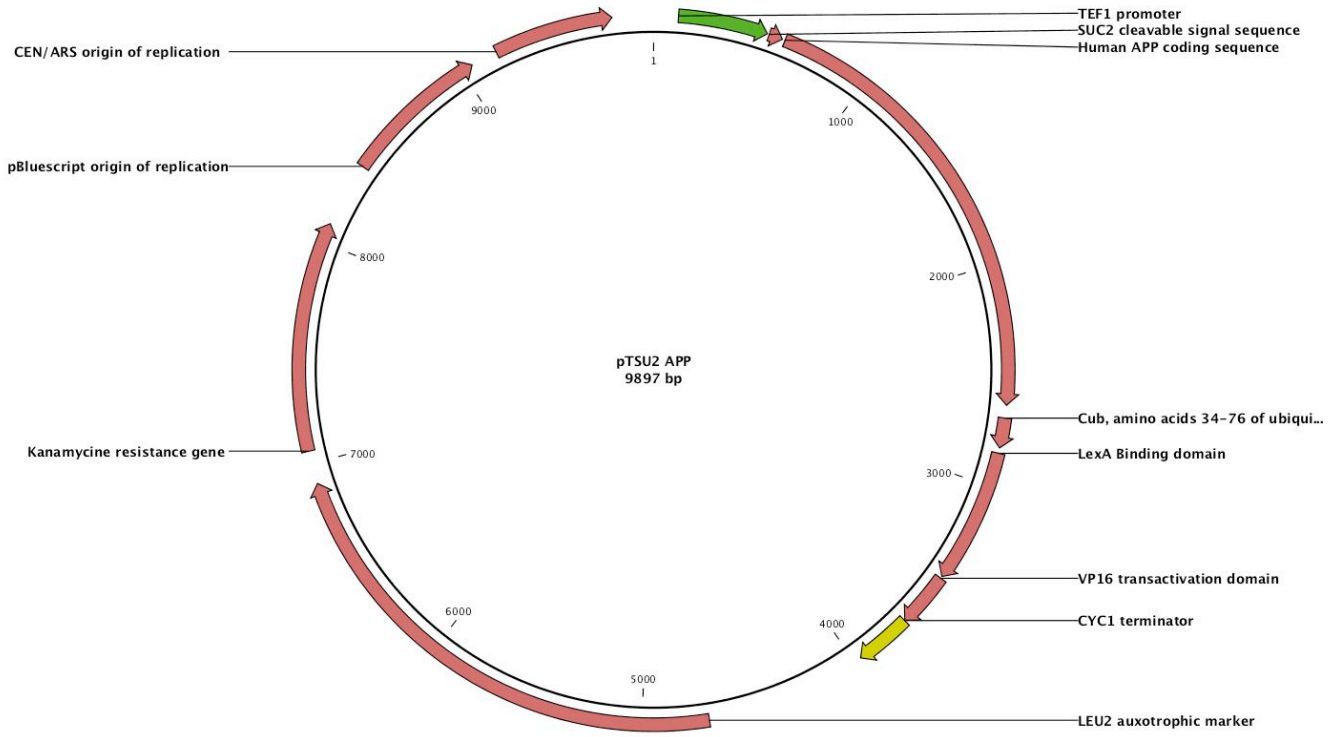

Figure 30. pTSU2APP Plasmid Map

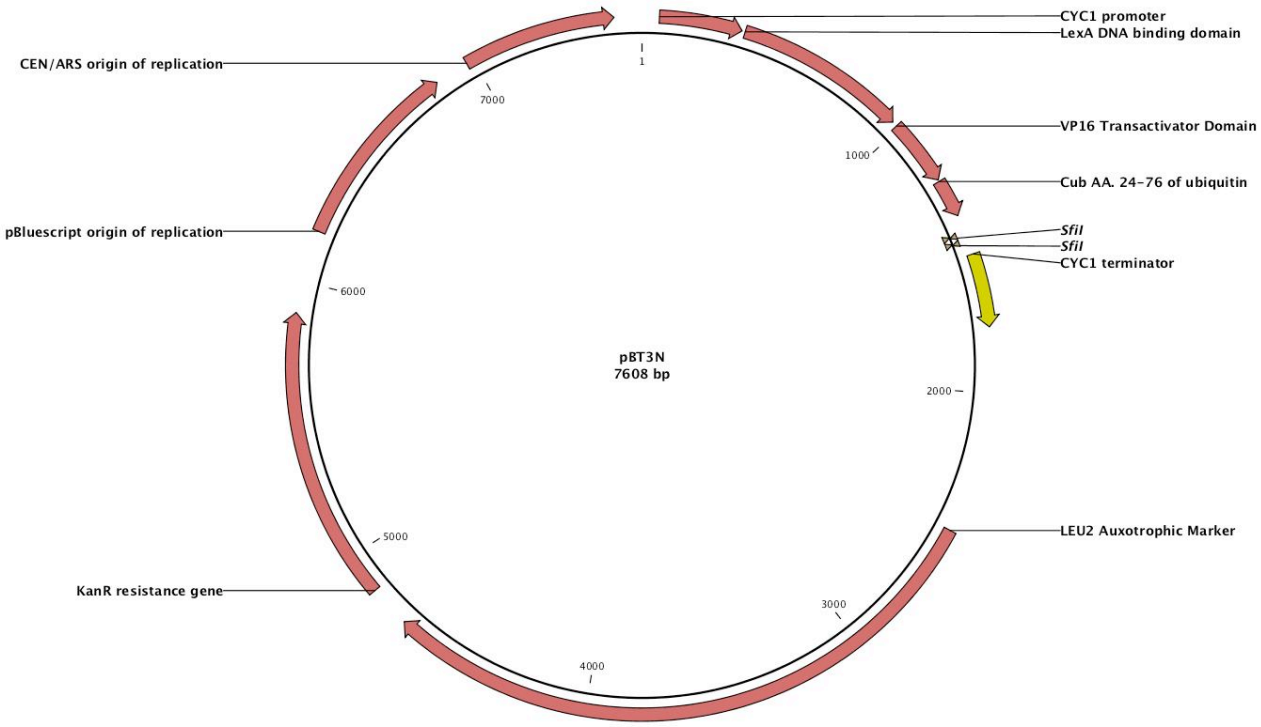

Figure 31. pBT3N Plasmid Map.

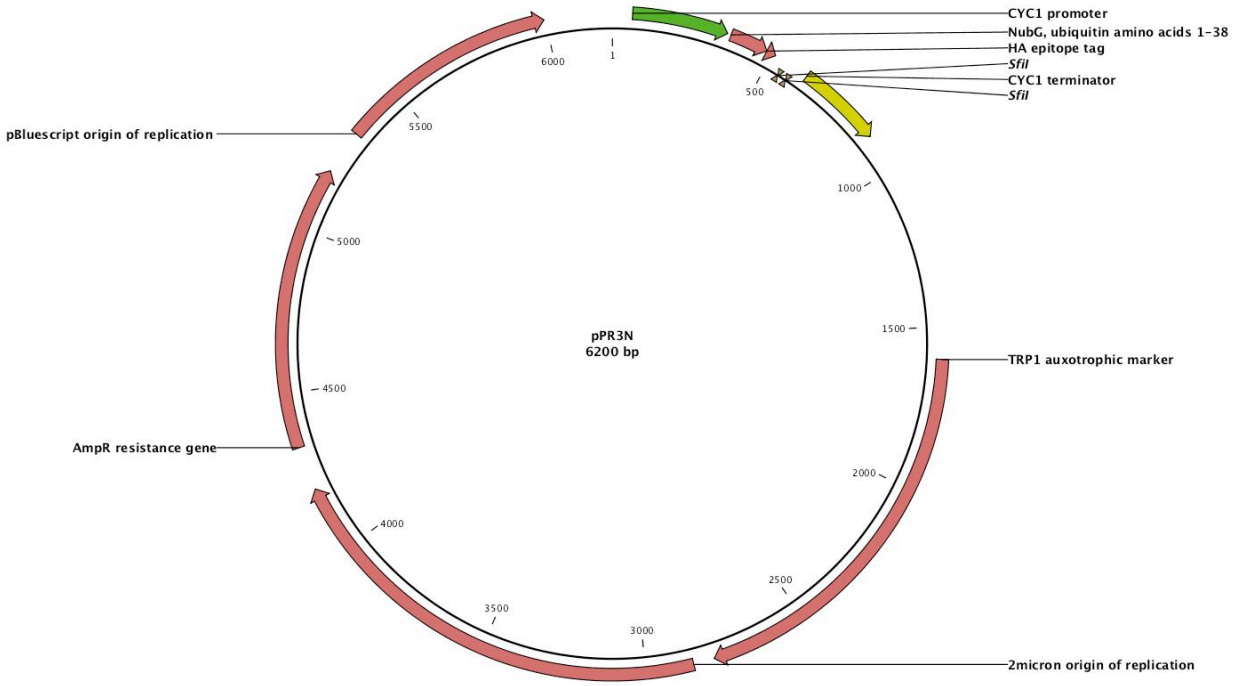

Figure 32. pPR3N Plasmid Map

9.0 List of Tables

Gene Cloned	Vector	Sequence Cloned	Cloning sites
Cesa 1	pENTR/D-Topo	cDNA	CACC
Cesa 3	pENTR/D-Topo	cDNA	CACC
Cesa 6	pENTR/D-Topo	cDNA	CACC
Cesa 3 Fpx 1-1 S(1040)L	pENTR/D-Topo	cDNA	CACC
Cesa 3 Fpx 1-2 S(1037)F	pENTR/D-Topo	cDNA	CACC
Cesa 3 Fpx 1-3 S(983)F	pENTR/D-Topo	cDNA	CACC
Cesa 1 Fpx 2-1 G(1013)R	pENTR/D-Topo	cDNA	CACC
Cesa 1Fpx 2-2 P(1010)L	pENTR/D-Topo	cDNA	CACC
Cesa 1 Fpx 2-3 G(1009)D	pENTR/D-Topo	cDNA	CACC
Aquaporin PIP2	pENTR/D-Topo	cDNA	CACC
Cesa 1	pPR3-N, pPR3-STE, pBT3-STE and pBT3-N	cDNA N/C Terminal Fusions	SfiI
Cesa 3	pPR3-N, pPR3-STE, pBT3-STE and pBT3-N	cDNA N/C Terminal Fusions	SfiI
Cesa 3 Fpx 1-1 S(1040)L	pPR3-STE	cDNA C-terminal Fusion	SfiI
Cesa 3 Fpx 1-2 S(1037)F	pPR3-STE	cDNA C terminal fusion	SfiI
Cesa 3 Fpx 1-3 S(983)F	pPR3-STE	cDNA C terminal fusion	SfiI
Det3	pPR3-STE	cDNA C terminal fusion	SfiI
Korrigan	pPR3-STE	cDNA C terminal fusion	SfiI
Pom1	pPR3-STE	cDNA C terminal fusion	SfiI

Table 1. List of Clones

Primer Name	Sequence
PIP2 Fwrd	5-CACCATGGCAAAGGATGTGGAA-3
PIP2 Rev	5-TTAGACGTTGGCAGCACTTC-3
cesa 3 rev	5-TCAACAGTTGATTCCACATTC-3
ZnCesa-F	5-CACCATGGAATCCGAAGGAGAA-3
cesa1 frwd	5-CACCATGGAGGCCAGTGCCGGC-3
cesa1 rev	5-CTAAAAGACACCTCCTTTGCC-3
cesa 6 frwd	5-CACCATGAACACCGGTGGTCGGTTA-3
cesa 6 rev2	5-TCACAAGCAGTCTAAACCACA-3

Table 2. Primer List for pENTR/D-TOPO Cloning

Primer Name	Sequence
RTactin71R	5-CCATGACACCAGTGTGCCTA-3
RTactin71F	5-AATGGTGAAGGCTGGTTTTG-3
RTCESA61R	5-GGACAAGCTTGATTGCCTTC-3
RTCESA61F	5-GTGGCATGTAACGAATGTGC-3
RTCESA31R	5-CTGGTTTTGCACTGAGGACA-3
RTCESA31F	5-GATCGTTTTGTGGCTTGTGA-3
RTCESA11R	5-CCCCTGTGTCGTCTGAATCT-3
RTCESA11F	5-GTCGCGTGTAATGAATGTGC-3

Table 3. Primer list for qRT-PCR

Primer Name	Sequence
cesa 3-6-	5-TGACACCAAGACAGAAGAACG-3
cesa 3-6+	5-TCCTCAGGTTTGACACCTCTC-3
cesa 1-9-	5-TTGGGTCCACATCTTCTTCC-3
cesa 1-9+	5-CGCGAGTATTTGGTTCATTC-3
cesa 1-3-	5-GAGTTCTTCGCCATTGGAAC-3
cesa 1-3+	5-AGCTAACAAGGCGAGACACC-3
pPR3-STE Fwrd Verification	5-TTTCTGCACAATATTTCAAGC-3
pPR3-STE Rev Verification	5-CTTGACGAAAATCTGCATGG-3
pPR3-NVeriffrwrd	5-GTCGAAAATTCAAGACAAGG-3
pPR3-NVerifRev	5-AAGCGTGACATAACTAATTAC-3
pBT3-NVerfFwrd	5-CAGAAGGAGTCCACCTTAC-3
pBT3-NVerifRev	5-AAGCGTGACATAACTAATTAC-3
pBT3STEVerifFwrd	5-TGGCATGCATGTGCTCTG-3
pBT3-STEVerifRev	5-GTAAGGTGGACTCCTTCT-3
M13 fwrd	Used by TCAG
M13 rev	Used by TCAG

Table 4. Plasmid List for Sequencing

Primer Name	Sequence
pBT3/PR3-N/STECesa1Fwrd	5-ATTAACAAGGCCATTACGGCCATGGAGGCCAGTGCCGGCTTG-3
pBT3/PR3-NCesa1Rev	5-AACTGATTGGCCGAGGCGGCCCTAAAAGACACCTCCTTTGCC-3
pBT3/PR3-NCesa3Fwrd	5-ATTAACAAGGCCATTACGGCCATGGAATCCGAAGGAGAAACC-3
pBT3/PR3-NCesa3Rev	5-AACTGATTGGCCGAGGCGGCCTCAACAGTTGATTCCACATTC-3
pBT3-STECesa1Rev	5-AACTGATTGGCCGAGGCGGCCCCAAAGACACCTCCTTTGCCATT-3
pPR3-Ncesa1glyadd	5-ATTAACAAGGCCATTACGGCCGGTATGGAGGCCAGTGCCGGCTTG-3
Cesa1pPR3-STEFrwd	5-ATTAACAAGGCCATTACGGCCTTATGGAGGCCAGTGCCGGCTTG -3
Cesa3pPR3-STEFwrd	5-ATTAACAAGGCCATTACGGCCTTATGGAATCCGAAGGAGAAAC-3
Cesa3pBT3-STE/pPR3-STERev	5-AACTGATTGGCCGAGGCGGCCCCACAGTTGATTCCACATTCCAG-3
Det3Fwrd	5-ATTAACAAGGCCATTACGGCCTTATGACTTCGAGATATTGG-3
Det3 Rev	5-AACTGATTGGCCGAGGCGGCCCCAGCAAGGTTGATAGTGAAG-3
Korrigan Fwrd	5-ATTAACAAGGCCATTACGGCCTTATGTACGGAAGAGATCCA-3
Korrigan Rev	5-AACTGATTGGCCGAGGCGGCCCCAGGTTTCCATGGTGCTGG-3
Pom1 Fwrd	5-ATTAACAAGGCCATTACGGCCTTATGGTGACAATCAGGAGTGG-3
Pom1 Rev	5-AACTGATTGGCCGAGGCGGCCCCCGAAGAGGAAGAGGAAGGTAC-3

Table 5. Plasmid List for MbyTH Cloning

Mutant (Pool number)	Next Gen Mapping	Sequencing C-terminal end of *CESA1 and CESA3*	Segregation Ratio	Designation	See figure
R19**		S(1040)L	N/A	*fpx 1-1*	***Fig. 7.***
32-1 32-2-1 50-2-1		S(983)F	Dominant at 20 nM	*fpx 1-3*	***Fig. 7.***
35-2	S(307)L	-	Dominant Epistatic 1:3:12 X^2=36.2, df=2 p<0.001	*fpx 2-4*	***Appendix Fig.36***
42-2 45-1	P(1010)L	P(1010)L	Recessive at all concentrations 1:3 X^2=8.92, df=1 0.001<p<0.01	*fpx 2-2*	***Fig. 8.***
45-2 43-1		G(1013)R	1:3 X^2=5.95, df=1 0.01<p<0.02	*fpx 2-1*	***Fig. 8.***
56-2		-	N/A		
60-2		-	N/A		
63		-	N/A		
66-1		S(1037)F	Dominant at 20 nM	*Fpx 1-2*	
66-2		-	N/A		
70-2-1	S(307)L	S(307)L	Recessive at all concentrations 1:3 X^2=5.86, df=1 0.01<p<0.02	*fpx 2-4*	***Appendix Fig.36***
70-3		-	N/A		
73-1	G(1009)D	G(1009)D	Recessive at all concentrations 1:3 X^2=6.23, df=1 0.01<p<0.02	*fpx 2-3*	***Fig. 8.***
85-2		-	N/A		

Table 6. Flupoxam screen summary. Mutant alleles either mapped through Next generation mapping or sequencing are shown, along with there designation. Segregation ratios of those available are provided with Chi-Squared values.

10.0 Appendix

10.1 Next-Generation Mapping of 70-2-1 and 35-2.

Two individuals *fpx* 70-2-1 and *fpx* 35-2 were backcrossed to Columbia to generate an F2 population and plated on 20 nM flupoxam. DNA was isolated from 50 individuals of and sent for Next Generation Sequencing. Chastity belt mapping pinpointed both mutations to Cellulose synthase 1. Unlike the others in the C-terminus, this mutation is a S(307)F in the N-terminus and annotated as *fpx* 2-4 (**Fig. 36.)**. 70-2-1 contained the S(307)F mutation alone while 35-2 appeared to have a secondary mutation that was difficult to locate. Segregation analysis show *Fpx* 35-2 displays a dominant epistatic relationship of 12:3:1 (sensitive : semiresistant : resistant. (**Fig. 35.)**. It was hypothesized that the original F2 population sent for sequencing contained a mix of heterozygotes for both potential genes, therefore obscuring the ability of the chastity statistic to locate the true mutations since a heterozygous individual would lower the discordant chastity statistic (the number of mutant alleles in the pool in comparison to the parental line). F2 individuals were re-selected at a higher concentration of 10 uM as opposed to 20 nM. The new data again pinned the mutation to the right arm of chromosome 4 containing S(307)F with a background secondary mutation somewhere within the large arm of chromosome 4. A short list of potential candidates are listed in **Table 8.** A membrane yeast two hybrid using CESA 1 as the bait and potential interactors may point to a potential CESA 1 interacting protein.

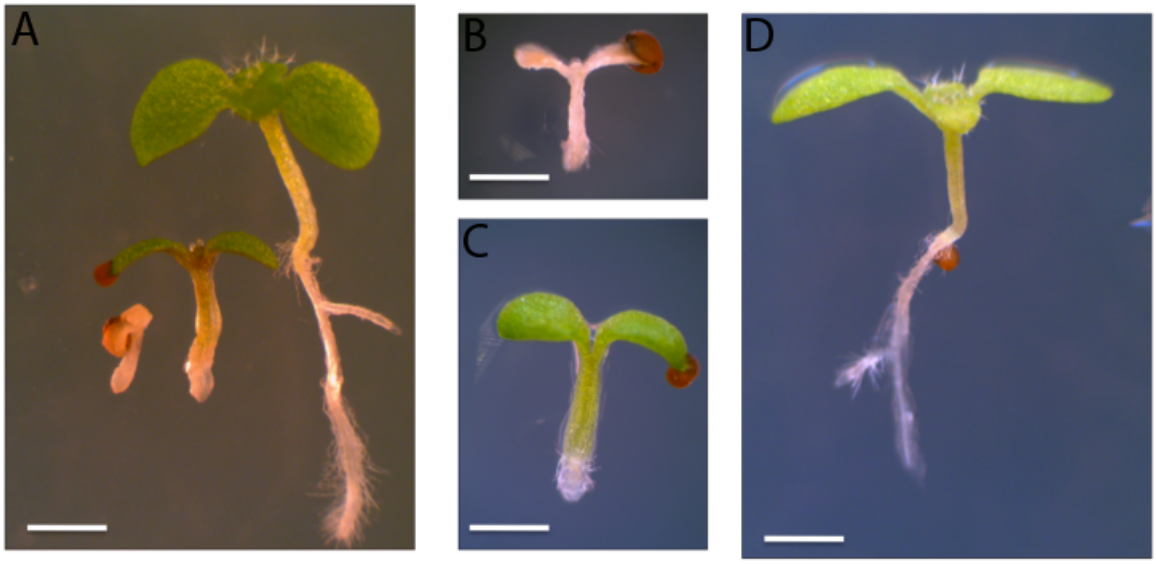

Figure 33. Segregation of 35-2 F2 Population on 10 uM flupoxam.

Segregation of 35-2 indicates the presence of two separate genes which display a dominant epistatic relationship (**A)** of 12:3:1 (sensitive **(B)** : semiresistant (**C)**: resistant **(D)**.

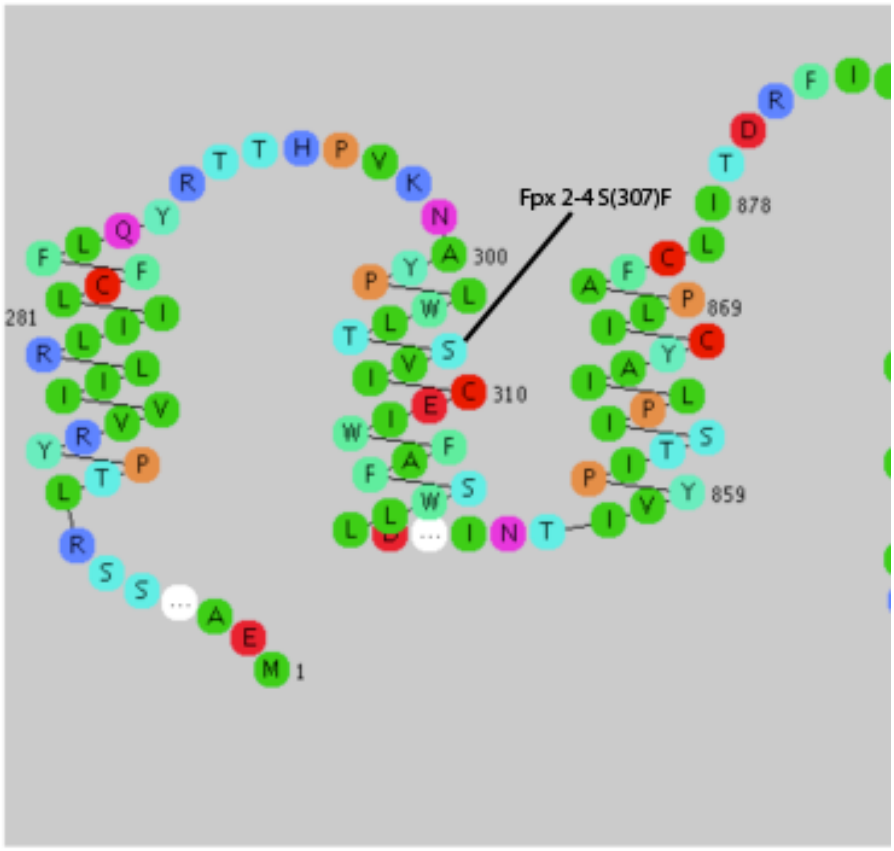

Figure 34. Residue Based Diagram Editor(RbDe) for N-Terminal Region of CESA1.

Mutation Fpx 2-4 S(307)F is indicated in the N-terminal region of CesA 1 (At4G32410).

AT4G27870	Vacuolar iron transporter (VIT) family protein
AT4G29250	HXXXD-type acyl-transferase family protein
AT4G32040	A member of Class II KN1-like homeodomain transcription factors factors
AT4G35240	Protein of unknown function (DUF630 and DUF632); INVOLVED IN: N-terminal protein myristoylation
AT4G35810	2-oxoglutarate (2OG) and Fe(II)-dependent oxygenase superfamily protein
AT4G36280	Histidine kinase-, DNA gyrase B-, and HSP90-like ATPase family protein; FUNCTIONS IN: ATP binding; INVOLVED IN: biological_process unknown
AT4G36350	Purple acid phosphatase 25 (PAP25); FUNCTIONS IN: protein serine/threonine phosphatase activity, acid phosphatase activity; INVOLVED IN: biological_process unknown

Table 7. A short list of potential gene candidates for 35-2